

1 **The influence of earthquake gates on surface rupture length**

2 **A.M. Rodriguez Padilla** ^{1,2*}, **M.E. Oskin**¹, **E.E. Brodsky**³, **K. Dascher-Cousineau**⁴, **V.**
3 **Herrera**⁵, **S. White**^{6,7}

4 ¹ Department of Earth and Planetary Sciences, University of California, Davis

5 ² Now at Division of Geological and Planetary Sciences, California Institute of Technology

6 ³ Department of Earth and Planetary Sciences, University of California, Santa Cruz

7 ⁴ Department of Earth and Planetary Sciences, University of California, Berkeley

8 ⁵ Department of Earth and Environmental Sciences, San Diego State University

9 ⁶ Geology Department, Pasadena City College

10 ⁷ Now at Department of Earth, Planetary, and Space Sciences, University of California, Los
11 Angeles

12
13 *Corresponding author: Alba M. Rodriguez Padilla (alba@caltech.edu,
14 amrodriguezpadilla@gmail.com)

15 **Key Points:**

- 16 ● We map step-overs, bends, gaps, splays, and strands from surface ruptures at 1:50,000
17 scale and assess their potential as earthquake gates
- 18 ● Step-overs wider than ~1.2 km and bends >30 degrees consistently halt propagating
19 ruptures, suggesting surficial complexity extends to depth
- 20 ● Our findings support that earthquake gates limit the size of large events

21
22
23
24
25

26 **Abstract**

27 Propagating earthquakes must overcome geometrical complexity on fault networks to grow
28 into large, surface rupturing events. We map step-overs, bends, gaps, splays, and strands of
29 length scales ~100-500 meters from the surface ruptures of 31 strike-slip earthquakes, recording
30 whether ruptures propagated past the feature. We find that step-overs and bends can arrest
31 rupture and develop a statistical model for passing probability as a function of geometry for each
32 group. Step-overs wider than 1.2 km, single bends larger than 32° , and double bends larger than
33 38° are breached by rupture half of the time. ~20% of the ruptures terminate on straight
34 segments. We examine how the distribution of earthquake gates influences surface rupture
35 length, inferring an exponential relationship between rupture length and event probability for a
36 given fault. Our findings support that earthquake gates limit the size of large events and help
37 discriminate between different proposed models of rupture propagation.

38

39

40 **Plain Language Summary**

41 Zones of geometrical complexity along faults can behave as barriers or earthquake gates that
42 sometimes halt propagating earthquakes. We map five types of geometrical complexities from
43 historical surface rupture maps and regional fault maps: step-overs, bends, gaps, splays, and
44 strands at 1:50,000 scale, corresponding to features >100-500 m in length. This is a finer scale
45 than previous studies, which focused on kilometer-scale zones of geometrical complexity. We
46 classify each mapped zone of geometrical complexity as breached (earthquake propagated past)
47 or unbreached (earthquake halted) and measure the width of step-overs and strands, the length of
48 gaps, and the angle of splays and bends. Based on these measurements, we model the probability
49 that each feature will be breached given its geometry. Step-overs wider than 1.2 km, single bends
50 larger than 32° , and double bends larger than 38° are breached by rupture half of the time. ~20%
51 of the ruptures terminate on straight segments. Using our probabilities, we show that the
52 presence and geometry of earthquake gates in the 100-500 m length scale plays a first-order
53 control on the low likelihood of large surface rupturing earthquakes.

54

55

56

57 Introduction

58 Earthquake surface ruptures are composed of fault segments bound by zones of
59 geometrical complexity (e.g., Wesnousky, 2006; Manighetti et al., 2007; Klinger, 2010; Perrin et
60 al., 2016; Hamling et al., 2017). These zones of geometrical complexity can act as earthquake
61 gates where the probability of rupture propagation is conditional on prior earthquake history,
62 rupture dynamics, material properties, and the stress conditions on neighboring fault segments.
63 For earthquakes on vertically dipping strike-slip faults, where the thickness of the seismogenic
64 zone limits down-dip rupture propagation, geometrical complexities have been proposed to exert
65 an important control on rupture length, and thus magnitude (e.g., Wesnousky, 2006).

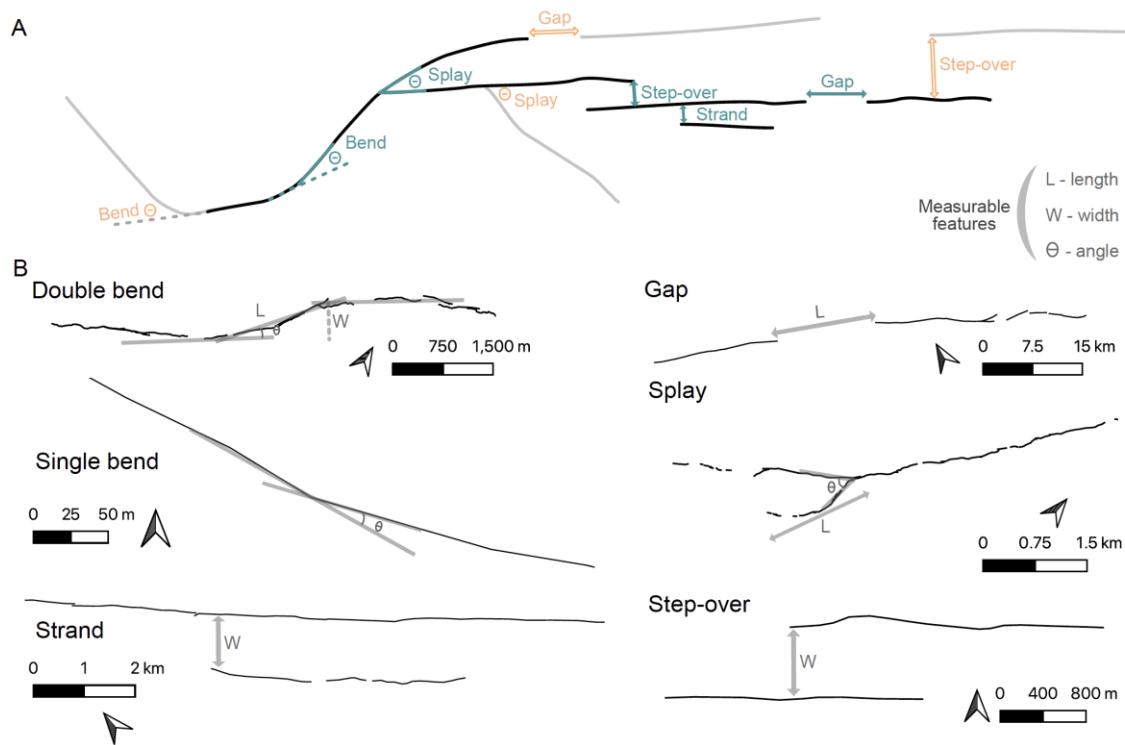
66 Historical earthquake rupture maps provide tests for geometrical controls on rupture
67 propagation that serve as validation for rupture simulator forecasts and dynamic rupture models
68 (e.g., Lettis et al., 2002; Wesnousky, 2006, 2008; Biasi and Wesnousky, 2016, 2017, 2021).
69 Most previous studies relied on simplified rupture maps, limiting the minimum size of
70 earthquake gates considered to kilometer-scale. This scale is practical for hazard applications, as
71 it is comparable to the resolution of complexity on regional fault maps and is commensurable
72 with model discretization in rupture simulators (Biasi and Wesnousky, 2021; Milner et al.,
73 2022).

74 Though limited in potential for prospective hazard assessment, observations suggest that
75 finer scale geometrical complexity can also exhibit earthquake gate behavior. For example, the
76 2014 Napa earthquake terminated in a 750-meter-wide step-over, too small to be included in
77 most previous studies. With new surface rupture maps from recent events, concurrent with
78 ongoing efforts to standardize past rupture maps (e.g., Sarmiento et al., 2021; Nurminen et al.,
79 2022) and improve regional fault maps, it is now possible to consider whether finer scale
80 geometrical complexity can act as an earthquake gate and how the distribution of this complexity
81 influences the probability of rupture propagation and final event size.

82 In this study, we map geometrical complexities at 1:50,000 scale, which corresponds with
83 features >100-500 meters in length scale, from 31 strike-slip surface rupture maps in the unified
84 Fault Displacement Hazard Initiative (FDHI) database (Sarmiento et al., 2021) and their
85 corresponding regional fault maps (see supplementary methods). We consider five types of
86 geometrical complexity: step-overs, bends, splays, gaps, and strands (Figure 1). Step-overs are
87 spaces between neighboring, parallel, overlapping faults. Bends are locations where the fault

88 changes strike. Bends may come in pairs (double bends) where the fault returns to its original
 89 orientation. Step-overs and double bends may be classified as a restraining (net contraction) or
 90 releasing (net extension), but single bends cannot be classified as such without knowledge of
 91 rupture propagation direction. Gaps are spaces between coplanar faults, distinct from step-overs,
 92 where faults are not coplanar. Splays are locations where the fault branches. We also consider
 93 fault strands that are parallel to subparallel of the continuous, main rupture that are activated
 94 without the rupture reaching the terminus of the main fault.

95 From our maps, we estimate the passing probabilities of the different features as a
 96 function of their geometry, characterizing their potential as earthquake gates. Using these
 97 probability distributions, we analyze the joint probability of the observed breached gates and
 98 straight segments for each event and characterize the relationship of these probabilities to the
 99 observed surface rupture length.



100
 101 **Figure 1.** Geometrical complexity mapped in this study. (a) Simplified cartoon showing the
 102 features characterized. The black lines denote the surface rupture whereas the light gray lines
 103 represent the regional faults that did not rupture during the event. The widths, lengths, and angles
 104 measured are shown in teal for the breached features and in orange for the unbreached features.
 105 (b) Examples of breached features from the FDHI rupture map database (Sarmiento et al., 2021).

106

107 What geometrical complexities act as earthquake gates?

108 We classify each mapped feature as breached or unbreached, depending on whether the
109 rupture propagated past the feature. To consider the size and geometry distribution of the
110 earthquake gates we map, we estimate empirical cumulative distribution functions (ECDFs) for
111 each population (Figure 2), separated into breached and unbreached groups, and restraining and
112 releasing categories when possible. We infer that features with statistically distinct breached and
113 unbreached populations are likely to act as earthquake gates, where passing probability is
114 conditional in part on geometry. We use the two-sample Kolmogorov-Smirnoff (KS) test to
115 assess whether different subset groups of an earthquake gate are statistically different. We use
116 the p-value derived from the test, which is the probability of rejecting the null hypothesis that
117 samples in the two subset groups were drawn from the same distribution. The convention here
118 for statistical significance is $p < 0.05$.

119 We mapped a total of 71 step-overs, where 26 are releasing and 45 are restraining. The
120 widest breached step-over is ~ 1.8 km wide and restraining. The breached and unbreached step-
121 over populations are distinct, though the restraining and releasing groups are statistically
122 indistinguishable (p-values of ~ 0.5 and 0.7 for breached and unbreached populations
123 respectively). We also map 7 strands, up to ~ 2 km away from the rupturing fault. We mapped a
124 total of 130 gaps, where only 5 were unbreached. The largest breached gap is ~ 15 km long.
125 Despite the low number of unbreached gaps mapped, the breached and unbreached ECDFs are
126 statistically distinct (p-value of 0.01). Mapping an unbreached gap requires the rupturing fault
127 and faults of parallel strike ahead of it to have been mapped in the regional map to a sufficient
128 resolution to include gaps in the fault system. The low number of unbreached gaps we map may
129 reflect the limited resolution of candidate, unactivated faults on available regional fault maps.

130 We map a total of 449 bends and analyze these separated into restraining versus
131 releasing, and single versus double categories (Figure 2). The largest breached single bend is
132 $\sim 47^\circ$ and the largest breached double bend is $\sim 42^\circ$. The breached and unbreached single and
133 double bends are statistically different ($p = 3 \times 10^{-17}$ and $p = 0.005$), but the breached restraining and
134 releasing populations are not (p-values of 0.1 and 0.7 for breached and unbreached respectively).

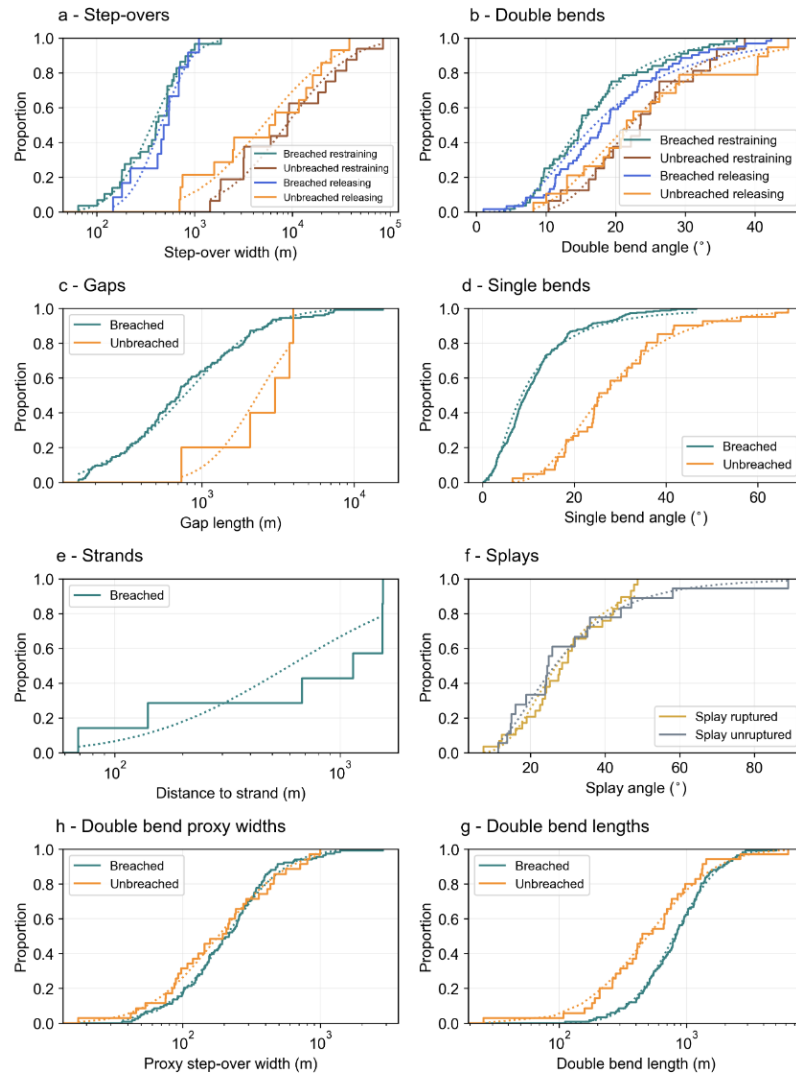
135 We map 47 splays. The angles of splays that were ruptured versus splays that were

136 bypassed cannot be separated by the KS test ($p=0.7$). In most cases where a splay was activated,
137 the rupture propagated less than 3 km onto the splay fault. Modeling studies suggest rupture
138 arrest at splays is related to the kinematics of the junction and the length of the fault branch
139 (Poliakov et al., 2002; Kame et al., 2004). Though we do not classify our splays into
140 transpressional or transtensional because the direction of rupture propagation is only known for
141 some events, the fact that we only observe two complete rupture arrests at splays suggests that
142 the presence of a splay plays a small role in the behavior of the rupture on the principal fault,
143 despite the fact that most splay branches mapped were relatively short, which should hinder
144 rupture propagation by allowing the two fault segments to interact as the rupture stops on the
145 shorter one (Bhat et al., 2007). Overall, our results suggest that splays do not play an important
146 role in rupture arrest at the mapping scale and that small splays may be surficial features without
147 depth-persistence.

148 An important difference between characterizing step-overs from simplified rupture maps
149 and the detailed rupture maps in the FDHI database is that the simplified rupture maps may not
150 include linking structures. Breached step-overs wider than 2 km measured in previous work (e.g.
151 Lettis et al., 2002) are hard-linked by faults in the more detailed rupture maps. We classify these
152 hard-linked steps as breached double bends or splays, depending on what feature achieves the
153 linkage. This is the case for the steps along the Landers earthquake which are hard linked by
154 splay faults and were previously described as “complex step-overs” (e.g., Biasi and Wesnousky,
155 2016).

156 As part of their evolution, step-overs can become hard-linked by fault segments, evolving
157 into double bends (Figure S1). We analyze our bend population by looking at two additional
158 geometrical characteristics, a bend length (Lozos et al., 2011), and a proxy step-over width
159 (Figure S1). When we parameterize bends by length or proxy step-over width, we find no clear
160 differences between the breached and unbreached populations (Figure 2h, g). This suggests that
161 step-overs that evolve into double bends become mechanically different features with higher
162 passing probability for the same (proxy) width. An important implication of this observation is
163 that the hard linkage we observe at the surface may persist at depth. This supports that
164 earthquake gates of small dimensions can span the entire seismogenic zone and play a role in
165 modulating rupture dynamics.

166 Rupture termination sometimes occurs on a straight portion of a fault, absent an observed
 167 earthquake gate, where the active fault continues for at least one kilometer past the rupture tip.
 168 This is the case for ~20% of the rupture termini in this study, comparable to the 10% of Biasi and
 169 Wesnousky (2016), who used a five-kilometer threshold for rupture continuation.



170

171 **Figure 2.** Empirical cumulative distribution function for the features mapped in this study (solid)
 172 and log-normal cumulative distribution fit for each ECDF (dotted). a: Restraining and releasing
 173 step-overs, parameterized based on width. b: Restraining and releasing double bends,
 174 parameterized based on angle. c: Gap length. d: Single bends, parametrized based on angle. e:
 175 Strands, parametrized based on their distance to the principal fault. f: Splays, separated into
 176 ruptured or unruptured and categorized by angle. g: Double bend proxy step-over width (Figures

177 1 and S1). h: Double bend length.

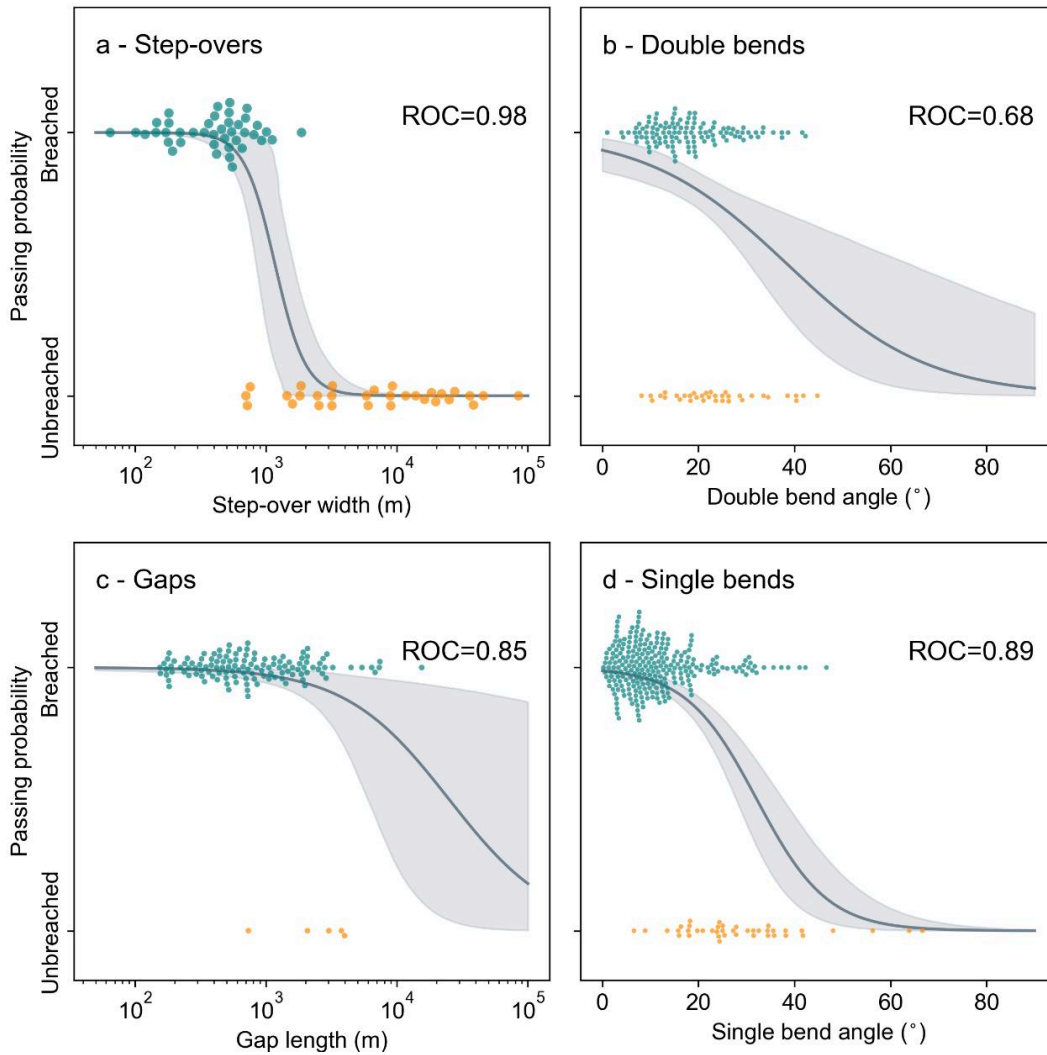
178 **Passing probabilities of earthquake gates**

179 Step-overs, gaps, and bends have statistically different breached and unbreached
180 populations, acting as earthquake gates. We estimate passing probability as a function of
181 geometry using a logistic model. This model describes the probability of a binary outcome
182 (breached versus unbreached) as a continuous function of the geometrical properties of an
183 earthquake gate, without requiring arbitrary binning of the data (see supplementary methods).
184 We use unweighted logistic regressions despite the number of features in the breached and
185 unbreached classes being different in the gaps and bends groups. We do this because, especially
186 for the bends, the range of breached and unbreached bend angles largely overlaps, so that the
187 relative frequency of breached and unbreached features is what distinguishes the two groups.
188 Weighting the data inversely by frequency would obscure this effect.

189 Because restraining and releasing features are not statistically different, we combine
190 these groups when estimating passing probabilities. Our logistic models (Figure 3) suggest that
191 step-overs wider than ~ 1.2 km will be breached less than half of the time. Step-overs >5 km will
192 be breached $<1\%$ of the time, consistent with the fact that they are not observationally
193 documented without linking structures in the rupture maps. The logistic models predict that
194 gaps longer than ~ 24.5 km will be breached less than half of the time. This distance is
195 considerably larger than for step-overs, which we interpret as evidence that the absence of
196 sufficient unbreached gap measurements precludes a robust estimate of passing probabilities for
197 gaps, or that gaps are not earthquake gates. Double bends $>38^\circ$ and single bends $>32^\circ$ are
198 predicted to be breached less than half of the time.

199 We assess the performance of our logistic regressions using an ROC score and confusion
200 matrix (Pedregosa et al., 2011, supplementary methods, Figures 3 and S3). Both metrics support
201 that step-over width is a strong predictor of rupture arrest. The logistic regressions struggle to
202 predict unbreached bends well. This is because the populations of breached and unbreached
203 bends largely span the same bend angles and are only separated by the changes in the breached
204 and unbreached frequency of that angle, which makes it difficult to predict with a binary
205 classifier. Therefore, at the mapping scale, only large bend angles ($>40^\circ$) consistently halt

206 earthquake ruptures.



207

208 **Figure 3.** Logistic regressions (gray) showing the passing probabilities of geometrical features.
 209 The data are shown as beehive plots, which show all data points in each classification, breached
 210 in teal and unbreached in orange. Restraining and releasing features are combined (shown
 211 separately in Figure S2). a: Passing probability as a function of step-over width. b: Passing
 212 probability as a function of double bend angle. c: Passing probability versus gap length. d:
 213 Passing probability as a function of single bend angle. The gray shading shows the 95%
 214 confidence interval calculated by bootstrapping.

215 Biasi and Wesnousky (2016) predict step-overs wider than 3 km will be breached <50%
 216 of the time. Three kilometers exceeds our largest observed breached step-over, which is ~1.8 km

217 wide. Biasi and Wesnousky (2017) also predict that bends sharper than 25° bend will be
 218 breached <50%. These findings are consistent with the estimate of Ozawa et al. (2023) using
 219 quasi-dynamic rupture models (Figure S4). We predict much larger passing probabilities of
 220 ~70% for single and double bends of that size. The differences between our passing probabilities
 221 and those in previous work arise from the use of different rupture maps (simplified versus not)
 222 and mapping at a finer scale. Mechanically, breaching the larger bends we map may require a
 223 locally heterogeneous stress field, as the large angle change would make the bend segment very
 224 incompatible with a uniform stress field, even at low static friction values (Biasi and Wesnousky,
 225 2017). A change in fault rake from strike-slip to dip-slip could also explain larger bend angles
 226 but we lack the data to test this option (see methods). Nevertheless, the fact that releasing and
 227 restraining features are statistically indistinguishable (Figure 2) is also consistent with a locally
 228 heterogeneous stress field, since homogeneous stress fields consistent yield distinctly different
 229 behavior for restraining and releasing features (e.g. Lozos et al., 2011).

230 Whether surficial fault geometry corresponds to that at depth is a challenge for using
 231 surface rupture maps to understand the physics of earthquake propagation. The different
 232 breached and unbreached populations and associated passing probabilities we obtain suggest a
 233 correlation between fault geometry at the surface and rupture propagation at depth. Together
 234 with the difference in rupture behavior through step-overs and double bends of the same
 235 dimensions, this suggests that the features we map at the surface, of 100-500 m length scales,
 236 extend downdip to the seismogenic zone.

237 **Geometrical controls on surface rupture length**

238 For each of the events examined, we model an event likelihood that reflects the pre-
 239 existing geometrical complexity in the hosting fault system as measured on the surface. We
 240 model event likelihood as the joint likelihood of continuing past the collective straight fault
 241 segments, $p(L)$, and breaching n gates each with passing probability p_i in an event: $P_{EQ} =$
 242 $P(L) \prod_{i=1}^N p_i$. We assume a constant chance of arrest at any point along without barriers and
 243 that the probabilities of stopping at different barriers are independent. Accordingly, the
 244 probability that segments reach a certain length in the absence of gates is the survival function of
 245 the exponential distribution, $p(L) = e^{-\lambda L}$ where L is the rupture length, and $\lambda = 1 \times$

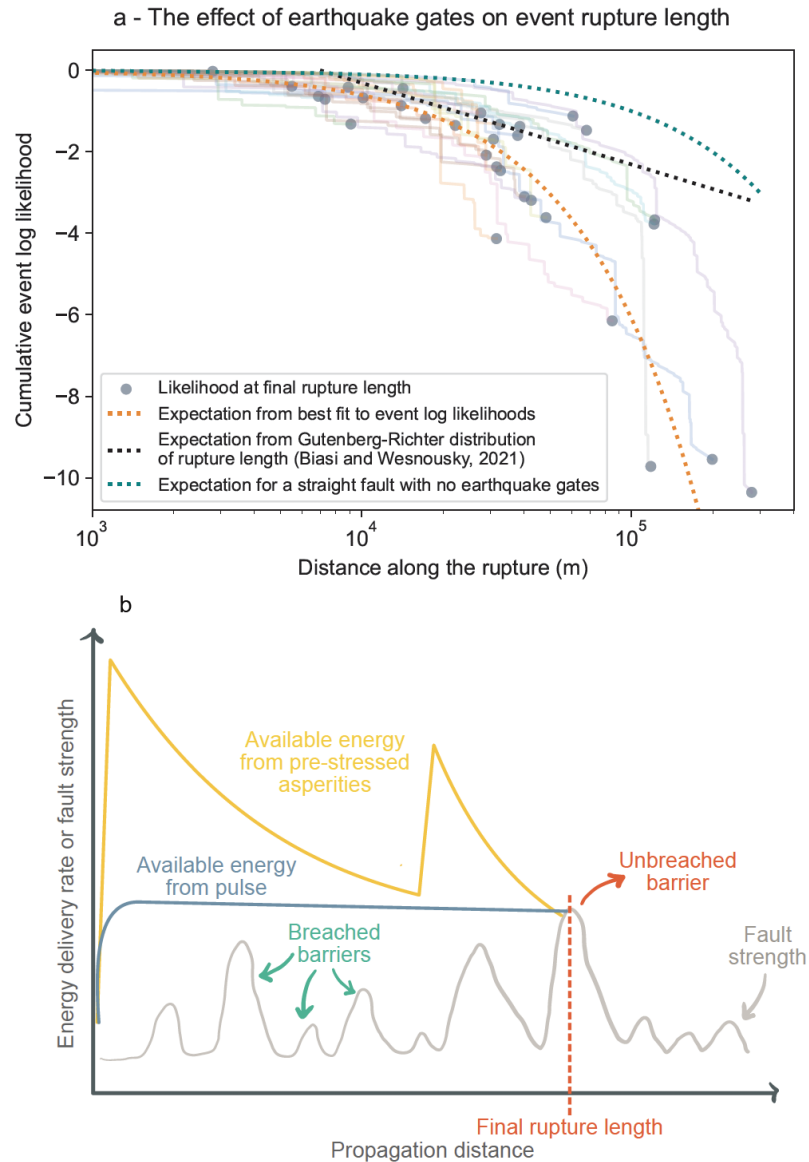
246 10^{-5} arrests/m is calculated by dividing the total number of arrests on straight segments by the
247 total rupture length of all events. We derive passing probabilities for each feature as a function of
248 its geometry from our logistic models (Figure 3). We exclude gaps from the likelihood estimates
249 given the small number of unbreached gaps sampled and the fact that they do not clearly behave
250 as gates.

251 To investigate the relationship of rupture length to event likelihood, we compute
252 likelihoods as cumulative probabilities along each mapped rupture (Figure 4a), following a
253 similar approach to Biasi and Wesnousky (2021). As ruptures encounter earthquake gates, the
254 cumulative log-likelihood of each event decreases. Because these ruptures are long, gates with
255 high passing probabilities contribute largely to reducing the event likelihood, even if their role in
256 rupture arrest is unlikely. The final likelihood of each event is well related to the rupture length
257 exponentially (Figure 4a), where the average spacing between neighboring gates is ~ 2 km
258 (Figure S5).

259 Earthquake scaling is typically considered in the context of the Gutenberg-Richter
260 relationship, which predicts a power-law relationship between event frequency and rupture
261 length (Figure 4a). Like in previous work on deriving probabilities from surface ruptures, the
262 likelihood-length relationship does not match this prediction (Biasi and Wesnousky, 2021). With
263 independent stopping probabilities at earthquake gates, as is inferred here, event likelihood will
264 follow an exponential relationship, as opposed to a power law. To produce a power-law
265 relationship would require that passing probabilities increase with rupture length, which is not
266 supported by the observed distribution of earthquake gates (Figures 4a and S5). The Gutenberg-
267 Richter relationship is defined for a population of earthquakes but may not fully describe the
268 behavior of individual faults. Instead, each fault appears to have its own set of earthquake gates
269 that contribute towards limiting rupture length. The possibility of non-Gutenberg-Richter
270 behavior on a single fault is well-supported in the geological literature for surface-rupturing
271 earthquakes (e.g. Schwartz and Coppersmith, 1984) but contrasts from the Gutenberg-Richter
272 behavior associated with small earthquakes on single faults (Shelley et al., 2016). The distinction
273 may have to do with the energetics of small versus seismogenic zone spanning events.

274 In this dataset, earthquakes often ended at barriers, where $\sim 80\%$ of the
275 rupture termini occurred at earthquake gates, supporting that barriers play a fundamental role in

276 rupture arrest (Aki, 1979, 1989; King and Nabelek, 1985; Klinger et al., 2006; Rockwell and
277 Klinger, 2013). The distribution of breached barriers documented here also provide guidance on
278 the appropriate model for rupture growth and propagation. An end-member model arising from
279 linear elastic fracture mechanics is a crack with a uniform pre-stress in an infinite space, where
280 the elastic energy delivery rate would increase with rupture propagation length (e.g., Freund,
281 1998). In this model, stronger barriers would be required to stop rupture with greater propagation
282 distance. We do not find a correlation between event size and barrier size, or barrier size along
283 the rupture (Figures S6, S7 and S8). Therefore, this end-member is likely not appropriate and
284 some heterogeneity in the stress field is required. An alternative crack-model with pre-stressed
285 asperities results in a variable energy delivery rate (Lay and Kanamori, 1981; Li et al., 2023).
286 Under this model, the available elastic energy is supplied by the asperities and decreases as the
287 rupture propagates into regions with smaller pre-stress (Figure 4b). Seismological evidence
288 supports that large surface rupturing events may be fueled by several asperities along the rupture
289 (e.g. Li et al., 2023). This model predicts that larger gates would be breached in proximity to
290 asperities, where the energy delivery rate is largest. We find no relationship between the
291 geometry of breached gates and the distance to the event epicenter or the amplitude of the
292 displacement, proxies for the locations of asperities (Figures S9 and S10), though the
293 displacement data is limited for older events and certain regions. Pulses offer a third alternative.
294 Ruptures tend to propagate as pulses once the seismogenic zone has been saturated (e.g. Heaton,
295 1990; Melgar and Hayes, 2017; Weng and Ampuero, 2019), which would result in a constant
296 energy release rate under a homogeneous stress field. This model is consistent with the lack of
297 correlation between breached gate size and location along the rupture, but incomplete, as some of
298 our observations require a heterogeneous pre-stress distribution (e.g., large breached bend angles
299 and indistinguishable releasing and restraining features). A propagating pulse encountering a
300 collection of asperities of variable size that provide a variable energy delivery rate can explain
301 both the observations requiring a heterogeneous pre-stress on the fault, and the absence of strong
302 spatial relationships for the distribution of breached earthquake gates on the fault. Dynamic
303 rupture models incorporating a distribution of earthquake gates similar to that described may
304 provide a future test of this hybrid model.



305

306 **Figure 4.** a: Cumulative event likelihood versus distance along the surface rupture. Each colored
 307 line represents one event. The scattered dots indicate the event likelihood at its final rupture
 308 length. The rupture lengths are based on the FDHI event coordinate system (ECS) reference lines
 309 (Sarmiento et al., 2021). The orange line represents the best fit to the final event likelihoods. The
 310 black line represents the predicted decrease in event likelihood with rupture length using the
 311 Gutenberg-Richter relationship for magnitude scaling. All likelihoods estimated using base e . b:
 312 Schematic cartoon of how an earthquake gate will bring rupture to arrest, conditional on the
 313 available elastic energy being lower than the strength of the barrier. Schematic elastic energy for
 314 a crack with two pre-stressed asperities and a pulse in a homogeneous stress field shown.

315 When an earthquake terminates at a barrier, elevated residual stresses, if not relaxed, can
316 promote rupture propagation past the barrier in a future event. This behavior is observed in
317 multi-cycle rupture models (e.g., Duan and Oglesby, 2006; Molina-Ormazabal et al., 2023),
318 laboratory experiments (Cebry et al., 2023), and inferred from the occurrence of aftershocks at
319 barriers where ruptures terminate (Aki, 1979). Earthquake gates may therefore act as a barrier
320 during an event, and as an asperity in a future one. The data in this study only permit assessing
321 the behavior of individual gates over one earthquake cycle, but considering the data together
322 offers insights into the frequency over which earthquake gates may act as an energy source,
323 overlapping with locations of high slip on the fault, or energy sinks, overlapping with locations
324 of low slip. We find that most of the large earthquake gates correspond with locations of low slip
325 (Figure S10), consistent with ubiquitous barrier behavior, though small gates span a wide range
326 of slip values. The very rare overlap of high slip values and unbreached earthquake gates
327 suggests that, while earthquake gates may also act as asperities, this relationship is not frequent
328 enough or the effect sufficiently large to stand out in our surface-rupture dataset. This is
329 consistent with recent experimental work by Cebry et al. (2023), which showed that a high
330 normal stress bump (a bend) behaved most frequently as a barrier but occasionally as an energy
331 source, or asperity.

332 **Conclusions**

333 We map step-overs, bends, gaps, splays, and strands along the surface rupture maps of 31
334 strike-slip earthquakes at 1:50,000 scale, labeling these features as breached and unbreached. We
335 use these measurements to fit a logistic model to each feature that estimates passing probabilities
336 as a function of geometry. Step-over width as measured at the surface is an excellent predictor of
337 arrest. Bend angle is a worse predictor, although the ratio of unbreached to breached bends
338 increases consistently with increasing bend angle. The fact that gates are preferred stopping
339 points provides evidence that the surficial features can persist to depth. A more direct test of this
340 idea is provided by the different behavior of step-overs and double bends of the same (proxy)
341 width, which suggests that step-overs persist as discrete unlinked fault strands at depth. Our
342 results call for models with geometrically complex faults consistent with our mapping scale to
343 explore what dynamic rupture conditions may match our passing probabilities.

344 We use earthquake gate passing probabilities in each event to build an empirical model
345 for the growth and arrest of large earthquakes given the complexity of the hosting fault system.
346 The cumulative event likelihood tabulated along rupture strike supports a barrier model as a
347 factor in controlling earthquake size, where relatively straight fault segments are bounded by
348 geometrical barriers that must be breached for the rupture to continue growing.

349 **Acknowledgments**

350 We are grateful for comments from Julian Lozos and Glenn Biasi. We thank Coby Abrahams,
351 Will Steindhart, Jean-Philippe Avouac, and Alexis Saez for suggestions and So Ozawa for
352 sharing his data. S.W., V.H., and A.M.R.P. benefitted from mentoring from Gaby Noriega.
353 A.M.R.P was supported by NASA FINESST award 80NSSC21K1634.

354

355 **Open Research**

356 The rupture maps are available from the FDHI database (Sarmiento et al., 2021), accessed
357 May 2022. Data can be accessed at <https://zenodo.org/records/11095762> and code can be
358 accessed at https://github.com/absrp/passing_probabilities_EQgates_strikeslip/releases/tag/v1.0.

359 **References**

- 360 1. Aki, K. (1979). Characterization of barriers on an earthquake fault. *Journal of*
361 *Geophysical Research: Solid Earth*, 84(B11), 6140-6148.
- 362 2. Aki, K. (1989). Geometric features of a fault zone related to the nucleation and
363 termination of an earthquake rupture. In *Proceedings of Conference XLV. Fault*
364 *Segmentation Controls of Rupture Initiation and Termination* (pp. 1-9).
- 365 3. Bachmanov, D.M., Trifonov, V.G., Kozhurin, A.I. and Zelenin E.A.: AFEAD v.2021
366 *Active Faults of Eurasia Database*, <https://doi.org/10.13140/RG.2.2.10333.74726>, 2021.
- 367 4. Biasi, G. P., & Wesnousky, S. G. (2016). Steps and gaps in ground ruptures: Empirical
368 bounds on rupture propagation. *Bulletin of the Seismological Society of America*, 106(3),
369 1110-1124.
- 370 5. Biasi, G. P., & Wesnousky, S. G. (2017). Bends and ends of surface ruptures. *Bulletin of*
371 *the Seismological Society of America*, 107(6), 2543-2560.
- 372 6. Biasi, G. P., & Wesnousky, S. G. (2021). Rupture passing probabilities at fault bends and

- 373 steps, with application to rupture length probabilities for earthquake early warning.
374 Bulletin of the Seismological Society of America, 111(4), 2235-2247.
- 375 7. Cebry, S. B., Sorhaindo, K., & McLaskey, G. C. (2023). Laboratory earthquake rupture
376 interactions with a high normal stress bump. *Journal of Geophysical Research: Solid*
377 *Earth*, 128(11), e2023JB027297.
- 378 8. Crone, A. J., Personius, S. F., Craw, P. A., Haeussler, P. J., & Staff, L. A. (2004). The
379 Susitna Glacier thrust fault: Characteristics of surface ruptures on the fault that initiated
380 the 2002 Denali fault earthquake. Bulletin of the Seismological Society of America,
381 94(6B), S5-S22.
- 382 9. Davy, P. (1993). On the frequency-length distribution of the San Andreas fault
383 system. *Journal of Geophysical Research: Solid Earth*, 98(B7), 12141-12151.
- 384 10. Duan, B., & Oglesby, D. D. (2006). Heterogeneous fault stresses from previous
385 earthquakes and the effect on dynamics of parallel strike-slip faults. *Journal of*
386 *Geophysical Research: Solid Earth*, 111(B5).
- 387 11. Field, E. H., Biasi, G. P., Bird, P., Dawson, T. E., Felzer, K. R., Jackson, D. D., ... &
388 Zeng, Y. (2015). Long-term time-dependent probabilities for the third Uniform California
389 Earthquake Rupture Forecast (UCERF3). *Bulletin of the Seismological Society of*
390 *America*, 105(2A), 511-543.
- 391 12. Field, E. H., Jordan, T. H., Page, M. T., Milner, K. R., Shaw, B. E., Dawson, T. E., ... &
392 Thatcher, W. R. (2017). A synoptic view of the third Uniform California Earthquake
393 Rupture Forecast (UCERF3). *Seismological Research Letters*, 88(5), 1259-1267.
- 394 13. Hamling, I. J., Hreinsdóttir, S., Clark, K., Elliott, J., Liang, C., Fielding, E., ... & Stirling,
395 M. (2017). Complex multifault rupture during the 2016 M_w 7.8 Kaikōura earthquake,
396 New Zealand. *Science*, 356(6334), eaam7194.
- 397 14. Heaton, T. H. (1990). Evidence for and implications of self-healing pulses of slip in
398 earthquake rupture. *Physics of the Earth and Planetary Interiors*, 64(1), 1-20.
- 399
- 400 15. King, G., & Nábělek, J. (1985). Role of fault bends in the initiation and termination of
401 earthquake rupture. *Science*, 228(4702), 984-987.
- 402 16. Klinger, Y., Michel, R., & King, G. C. (2006). Evidence for an earthquake barrier model
403 from Mw~7.8 Kokoxili (Tibet) earthquake slip-distribution. *Earth and Planetary Science*

- 404 Letters, 242(3-4), 354-364.
- 405 17. Klinger, Y. (2010). Relation between continental strike-slip earthquake segmentation and
406 thickness of the crust. *Journal of Geophysical Research: Solid Earth*, 115(B7).
- 407 18. Langridge, R. M., Ries, W. F., Litchfield, N. J., Villamor, P., Van Dissen, R. J., Barrell,
408 D. J. A., ... & Stirling, M. W. (2016). The New Zealand active faults database. *New
409 Zealand Journal of Geology and Geophysics*, 59(1), 86-96.
- 410 19. Lay, T., & Kanamori, H. (1981). An asperity model of large earthquake
411 sequences. *Earthquake prediction: An international review*, 4, 579-592.
- 412 20. Lettis, W., Bachhuber, J., Witter, R., Brankman, C., Randolph, C. E., Barka, A., ... &
413 Kaya, A. (2002). Influence of releasing step-overs on surface fault rupture and fault
414 segmentation: Examples from the 17 August 1999 Izmit earthquake on the North
415 Anatolian fault, Turkey. *Bulletin of the Seismological Society of America*, 92(1), 19-42.
- 416 21. Lienkaemper, J. J., Pezzopane, S. K., Clark, M. M., & Rymer, M. J. (1987). Fault
417 fractures formed in association with the 1986 Chalfant Valley, California, earthquake
418 sequence: preliminary report. *Bulletin of the Seismological Society of America*, 77(1),
419 297-305.
- 420 22. Li, J., Kim, T., Lapusta, N., Biondi, E., & Zhan, Z. (2023). The break of earthquake
421 asperities imaged by distributed acoustic sensing. *Nature*, 620(7975), 800-806.
- 422 23. Lozos, J. C., Oglesby, D. D., Duan, B., & Wesnousky, S. G. (2011). The effects of
423 double fault bends on rupture propagation: A geometrical parameter study. *Bulletin of the
424 Seismological Society of America*, 101(1), 385-398.
- 425 24. Manighetti, I., Campillo, M., Bouley, S., & Cotton, F. (2007). Earthquake scaling, fault
426 segmentation, and structural maturity. *Earth and Planetary Science Letters*, 253(3-4),
427 429-438.
- 428 25. Melgar, D., & Hayes, G. P. (2017). Systematic observations of the slip pulse properties of
429 large earthquake ruptures. *Geophysical Research Letters*, 44(19), 9691-9698.
- 430 26. Milner, K. R., Shaw, B. E., & Field, E. H. (2022). Enumerating plausible multifault
431 ruptures in complex fault systems with physical constraints. *Bulletin of the Seismological
432 Society of America*, 112(4), 1806-1824.
- 433 27. Molina-Ormazabal, D., Ampuero, J. P., & Tassara, A. (2023). Diverse slip behaviour of
434 velocity-weakening fault barriers. *Nature Geoscience*, 16(12), 1200-1207.

- 435 28. Nurminen, F., Baize, S., Boncio, P., Blumetti, A. M., Cinti, F. R., Civico, R., & Guerrieri,
 436 L. (2022). SURE 2.0—New release of the worldwide database of surface ruptures for fault
 437 displacement hazard analyses. *Scientific Data*, 9(1), 729.
- 438 29. Ozawa, S., Ando, R., & Dunham, E. M. (2023). Quantifying the probability of rupture
 439 arrest at restraining and releasing bends using earthquake sequence simulations. *Earth
 440 and Planetary Science Letters*, 617, 118276.
- 441 30. Pedregosa, F., Varoquaux, G., Gramfort, A., Michel, V., Thirion, B., Grisel, O., ... \&
 442 Duchesnay, E. (2011). Scikit-learn: Machine learning in Python. *the Journal of machine
 443 Learning research*, 12, 2825-2830.
- 444 31. Perrin, C., Manighetti, I., Ampuero, J. P., Cappa, F., & Gaudemer, Y. (2016). Location of
 445 largest earthquake slip and fast rupture controlled by along-strike change in fault
 446 structural maturity due to fault growth. *Journal of Geophysical Research: Solid Earth*,
 447 121(5), 3666-3685.
- 448 32. Rockwell, T. K., & Klinger, Y. (2013). Surface rupture and slip distribution of the 1940
 449 Imperial Valley earthquake, Imperial fault, southern California: Implications for rupture
 450 segmentation and dynamics. *Bulletin of the Seismological Society of America*, 103(2A),
 451 629-640.
- 452 33. Sarmiento, A., Madugo, D., Bozorgnia, Y., Shen, A., Mazzoni, S., Lavrentiadis, G.,
 453 Dawson, T., Madugo, C., Kottke, A., Thompson, S., Baize, S., Milliner, C., Nurminen,
 454 F., Boncio, P., and Visini, F. (2021). Fault Displacement Hazard Initiative Database,
 455 UCL B. John Garrick Institute for the Risk Sciences, Report GIRS-2021-08, doi:
 456 10.34948/N36P48.
- 457 34. Schwartz, D. P., & Coppersmith, K. J. (1984). Fault behavior and characteristic
 458 earthquakes: Examples from the Wasatch and San Andreas fault zones. *Journal of
 459 Geophysical Research: Solid Earth*, 89(B7), 5681-5698.
- 460 35. Shelly, D. R., Ellsworth, W. L., & Hill, D. P. (2016). Fluid-faulting evolution in high
 461 definition: Connecting fault structure and frequency-magnitude variations during the
 462 2014 Long Valley Caldera, California, earthquake swarm. *Journal of Geophysical
 463 Research: Solid Earth*, 121(3), 1776-1795.
- 464 36. Styron, R., & Pagani, M. (2020). The GEM global active faults database. *Earthquake
 465 Spectra*, 36(1), 160-180.

- 466 37. U.S. Geological Survey, 2020, Quaternary Fault and Fold Database for the Nation,
467 accessed [August, 10, 2022], at <https://doi.org/10.5066/P9BCVRCK>
- 468 38. Wells, D. L., & Coppersmith, K. J. (1993). Likelihood of surface rupture as a function of
469 magnitude. *Seismological Research Letters*, 64(1), 54.
- 470 39. Wechsler, N., Ben-Zion, Y., & Christofferson, S. (2010). Evolving geometrical
471 heterogeneities of fault trace data. *Geophysical Journal International*, 182(2), 551-567.
- 472 40. Weng, H., & Ampuero, J. P. (2019). The dynamics of elongated earthquake
473 ruptures. *Journal of Geophysical Research: Solid Earth*, 124(8), 8584-8610.
- 474 41. Wesnousky, S. G. (1988). Seismological and structural evolution of strike-slip faults.
475 *Nature*, 335(6188), 340-343.
- 476 42. Wesnousky, S. G. (2006). Predicting the endpoints of earthquake ruptures. *Nature*,
477 444(7117), 358-360.
- 478 43. Wesnousky, S. G. (2008). Displacement and geometrical characteristics of earthquake
479 surface ruptures: Issues and implications for seismic-hazard analysis and the process of
480 earthquake rupture. *Bulletin of the Seismological Society of America*, 98(4), 1609-1632.

Geophysical Research Letters

Supporting Information for

The influence of earthquake gates on surface rupture length

**A.M. Rodriguez Padilla^{1,2*}, M.E. Oskin¹, E.E. Brodsky³, K. Dascher-Cousineau⁴, V.
Herrera⁵, S. White^{6,7}**

¹ Department of Earth and Planetary Sciences, University of California, Davis

² Now at Division of Geological and Planetary Sciences, California Institute of Technology

³ Department of Earth and Planetary Sciences, University of California, Santa Cruz

⁴ Department of Earth and Planetary Sciences, University of California, Berkeley

⁵ Department of Earth and Environmental Sciences, San Diego State University

⁶ Geology Department, Pasadena City College

⁷ Now at Department of Earth, Planetary, and Space Sciences, University of California, Los Angeles

*Corresponding author: Alba M. Rodriguez Padilla (alba@caltech.edu,
amrodriguezpadilla@gmail.com)

Contents of this file

Supplementary Methods

Figures S1 to S43

Tables S1 to S6

Introduction

This file contains the mapping method followed, supplementary figures S1 to S43, tables S1-S6, and the maps of each event and its corresponding earthquake gate. The maps are generated in 30 x 30 in files at 300 dpi so that they can be easily zoomed into and examined.

Supplementary Methods

Earthquake Gate Mapping

We choose to focus on strike-slip events because vertically dipping faults tend to remain constant in dip with depth so that surface geometry, besides fine-scale heterogeneity, can be used

31 as a proxy for the geometry at depth. We rely on the surface rupture maps compiled in the Fault
32 Displacement Hazard Initiative (FDHI) database (Sarmiento et al., 2021). At the time of access for
33 this manuscript (May, 2022), the database encompassed sixty-six, globally distributed, surface
34 rupturing earthquakes (M_w 5-8), of which thirty-one are strike-slip. The database includes surface
35 rupture maps for each event, where ruptures are classified as primary or distributed, displacement
36 measurements, and additional information, such as lithology or slope. Surface ruptures are mapped
37 to 1-meter precision in the database, though individual maps differ in the level of detail captured
38 in the surface rupture. This variability is in part related to the different degrees of complexity in
39 the hosting fault system, and in part a result of differences in mapping methods and extent across
40 ruptures.

41 We map earthquake gates from the surface ruptures in the FDHI database at a 1:50,000
42 scale, which roughly corresponds to mapping features with lengths exceeding 100-500 meters. At
43 this scale, we expect the level of detail across ruptures to be roughly comparable. The surface
44 rupture maps in the FDHI database include ruptures classified as principal and distributed. To
45 ensure that we only include primary faults, which are the seismogenic structures in the events in
46 our analysis, we consider the ruptures characterized as principal in the database. This also allows
47 for comparison across events with different spatial coverage of the off-fault deformation field.

48 Prior work has either relied on simplified rupture maps (e.g., Wesnousky, 2006) or
49 simplified ruptures to segments long enough (~ 7 km) to make results commensurable with
50 UCERF3 model discretization and comparable to standard fault maps (Biasi and Wesnousky,
51 2017, 2021). We map earthquake gates directly from the surface rupture maps, without simplifying
52 the rupture traces. An important consequence of our scale of choice (1:50,000) is that larger
53 features (for example, the large, regional-scale releasing bend in the Balochistan earthquake which
54 spans 6 km) are mapped into its smaller constituents that occur at the mapping scale (i.e. several
55 shorter bends that make up the regional one). Our scale of choice results in the mapping of smaller
56 step-overs that were previously not classified in prior work due to their small size but does not
57 influence the maximum breached step-over width that can be measured as long as the step is not
58 hard-linked, in which case it would be mapped as a bend or a splay.

59 We characterize gates as restraining or releasing when possible, depending on the
60 volumetric deformation fostered by the type of slip and the geometry of the fault segments. To do
61 this, we assume all fault segments involved in the rupture have strike-slip kinematics consistent

62 with the focal mechanism for the event. At large scales, this is a reasonable approximation for all
63 the strike-slip ruptures in the FDHI database except for the Denali earthquake, from which we
64 remove the portion of the rupture that occurred on the Susitna Glacier Thrust, where the earthquake
65 initiated (e.g., Crone et al., 2004). However, at finer scales, including our mapping scale,
66 transitions from strike-slip to more oblique or vertical slip can lead to larger bend angles. We do
67 not account for this limitation due to the absence of information to do so consistently for all events,
68 following the rationale of Biasi and Wesnousky (2017).

69 A portion of the Kobe earthquake ruptured offshore and is not available in our map, with
70 the section being onshore also being only a partial rupture to the surface, resulting in comparatively
71 short surface rupture for the event magnitude. Incomplete rupture to the surface is also a limitation
72 that applies to the smaller magnitude events considered here, such as the Chalfant Valley
73 earthquake.

74 We characterize five different types of earthquake gates in this study: step-overs, gaps,
75 bends, splays, and strands (Figure 1). We distinguish between breached features where the rupture
76 transferred through and continued for at least 1 kilometer, and unbreached features, where the
77 rupture halted immediately or within 1 km past the gate. For the case of splays, we classify cases
78 where the rupture transferred onto a splay (regardless of whether it also continued on the main
79 fault), as ruptured and instances where an available intersecting splay fault was foregone as
80 unruptured. Note the use of different terminology from breached and unbreached to indicate that
81 at least one fault strand was always active past the splay (Figure 1).

82 For each of the gates of interest, we measure the relevant geometrical attribute. For bends
83 and splays, this is the bend angle, which is the difference between the fault strike as it enters the
84 feature and the fault strike as it exits the feature. In the case of multi-stranded bends, we map the
85 bend strand with the smallest angle. We distinguish between single bends, where the fault strike
86 changes once, and double bends, where the fault strike changes for a segment and then returns to
87 the original strike (see examples in Figure 1). Because natural double bends have angles that are
88 not perfectly identical on each side of the bend limb, we take the average of the two angles. In
89 most cases, the angle difference between the two angles is well below 10 degrees. Step-overs occur
90 where a fault ends and the rupture is forced to jump onto a neighboring segment or come to arrest.
91 We also map locations where the rupture activates parallel to subparallel neighboring fault strands
92 without reaching the terminus of the principal fault. By definition, strands may only exist as

93 breached features, as there was no fault terminus that forced a jump. For step-overs and strands,
94 we measure the distance between parallel or subparallel fault segments at their minimum,
95 orthogonal to the fault segments when possible. For gaps, we measure the length of the gap
96 between the active rupture and another fault, or between parts of the active rupture if breached, in
97 the fault-parallel direction. Note that we do not have the ability to distinguish gaps that represent
98 pauses on the rupture on the same fault versus gaps that represent the spacing between two
99 sequential faults of parallel strike.

100 We rely on different active fault databases to characterize unbreached features, where we
101 measure the angle or distance between the ruptured fault and unruptured active faults in the
102 database. The reference databases we use are listed in Supplementary Table S1. For the United
103 States, the resolution of the regional faults associated with the events in this study in the Qfaults
104 database is comparable to the resolution of the primary rupturing faults in the FDHI database. For
105 the Darfield event in New Zealand, we use the NZAFD database, mapped at 1:250,000 (Langridge
106 et al., 2016). The Active Faults of Eurasia Database (AFEAD) database for Eurasia, which we use
107 for events in Turkey and Asia, is mapped at 1:500,000 scale (Bachmanov et al., 2021). Last, the
108 GEM database, which we use only for the San Miguel and Pisayambo earthquakes in Mexico and
109 Ecuador respectively, is mapped at 1:1,000,000 scale (Styron and Pagani, 2020). In the interest of
110 classifying unbreached features as restraining or releasing, when the inactive fault kinematics are
111 unknown, we assume these are the same as the rupturing faults'. When two unbreached step-overs
112 may be measured at a fault's terminus, we map both, following the choice of previous workers
113 (e.g., Wesnousky, 2006). Note that some events (e.g., Galway Lake and Ridgecrest foreshock)
114 have unbreached step-overs at both of their termini with the same fault (e.g., the faults in the
115 Landers event and the Garlock fault respectively), in which case both unbreached step-overs are
116 mapped. When a gap and a step-over of the same size exist, and one gets breached but the other
117 one does not, we map both the breached and unbreached features. The same occurs where there is
118 a bend but the rupture instead skips the bend and jumps ahead to a more straight portion of the
119 fault. This only occurs in the case of very similarly sized earthquake gates available at the same
120 location, otherwise, we only map the smallest gate present. We provide our mapped earthquake
121 gates as shapefiles (see data availability section) and shown over the rupture maps and regional
122 fault maps in this supplementary section.

123

124 **Passing Probability and Event Likelihood Estimates**

125 To determine whether the forms of geometrical complexity we map (Figure 1) act as
126 barriers to rupture propagation, we analyze the distribution of breached and unbreached gates in
127 terms of the geometrical attribute measured (angle or length). We look at the cumulative
128 distribution functions of breached and unbreached gates and use a Kolmogorov-Smirnoff (KS) test
129 to determine whether the breached and unbreached populations are statistically different.

130 For those features where the breached and unbreached populations are statistically different
131 (Figure 2), we compute passing probabilities as a function of the geometrical characteristics of the
132 gate. To do so, we use a logistic function, which describes the probability of a binary outcome
133 (breached or unbreached) as a continuous function of the geometry of an earthquake gate. To fit
134 logistic regressions through our data, we use the Python package scikit learn (Pedregosa et al.,
135 2011). An advantage of using logistic regressions over past methods is that estimating probabilities
136 does not rely on arbitrary binning of the data. We evaluate the performance of our logistic models
137 for each type of earthquake gate using Receiver Operating Characteristic (ROC) scores and
138 confusion matrices, which is standard procedure for these models (Pedregosa et al., 2011). ROC
139 scores can range from 0.5 to 1, with increasing values indicating that more data points have been
140 correctly predicted by the logistic regression.

141

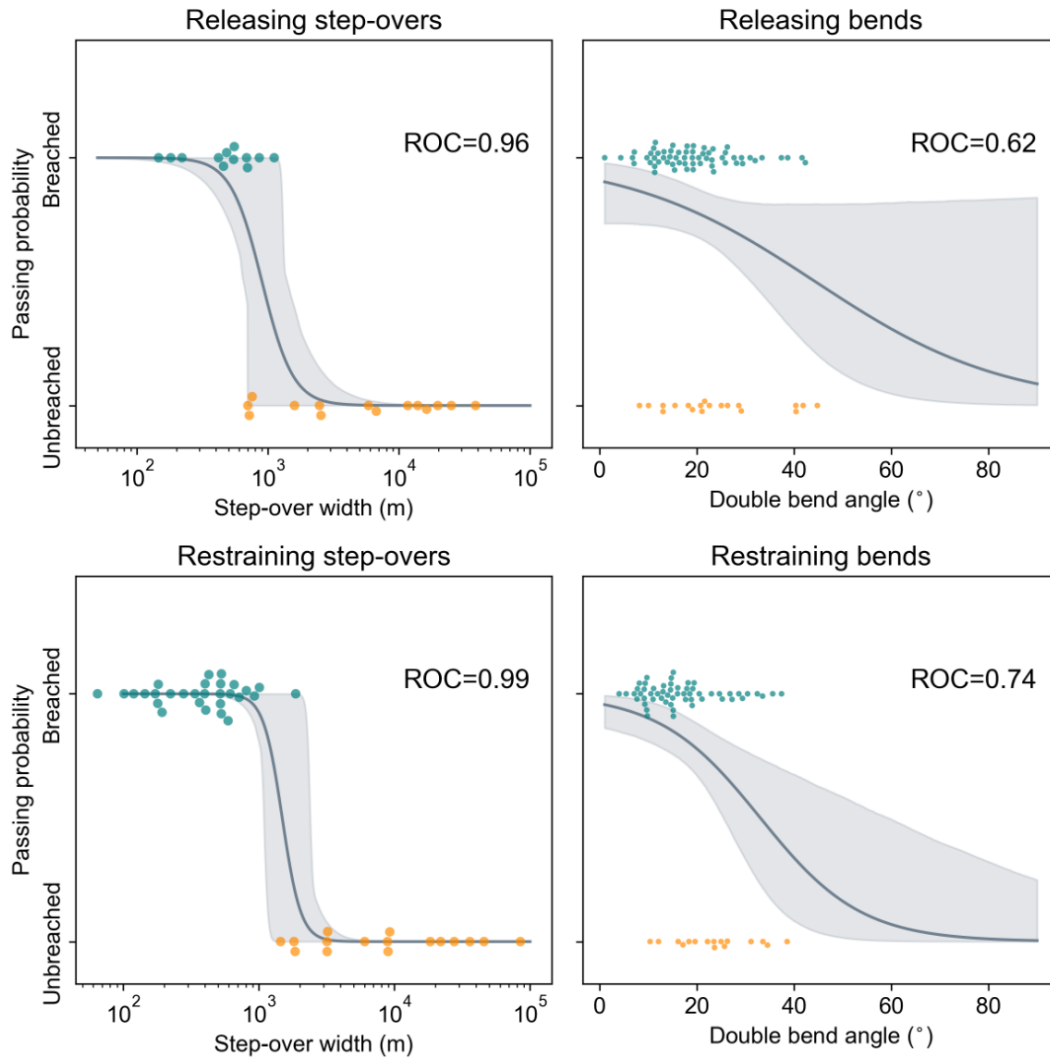
142

143 **Supplementary Figures**



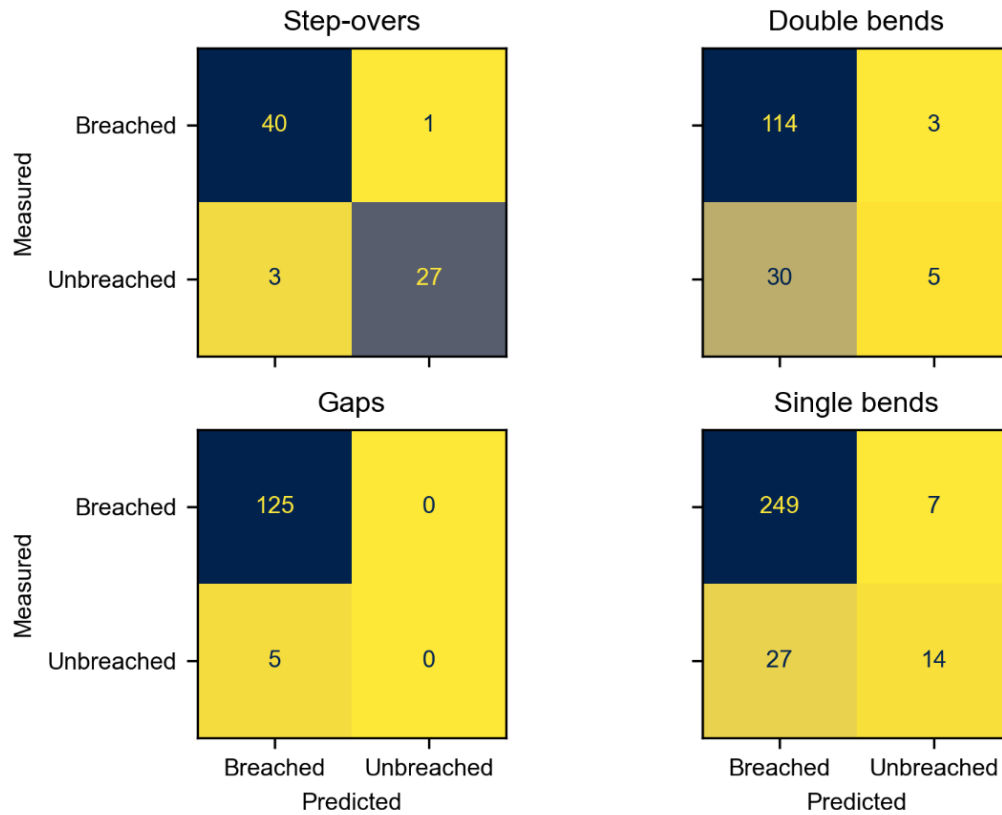
144

145 **Figure S1.** Releasing double bend from the 2014 Yutian earthquake. The rupture map is shown in
146 gray. The pink and purple lines show the bend length as defined by Lozos et al. (2011) and the
147 proxy step-over width respectively. The proxy step-over width is ~ 2.5 km wide.



148

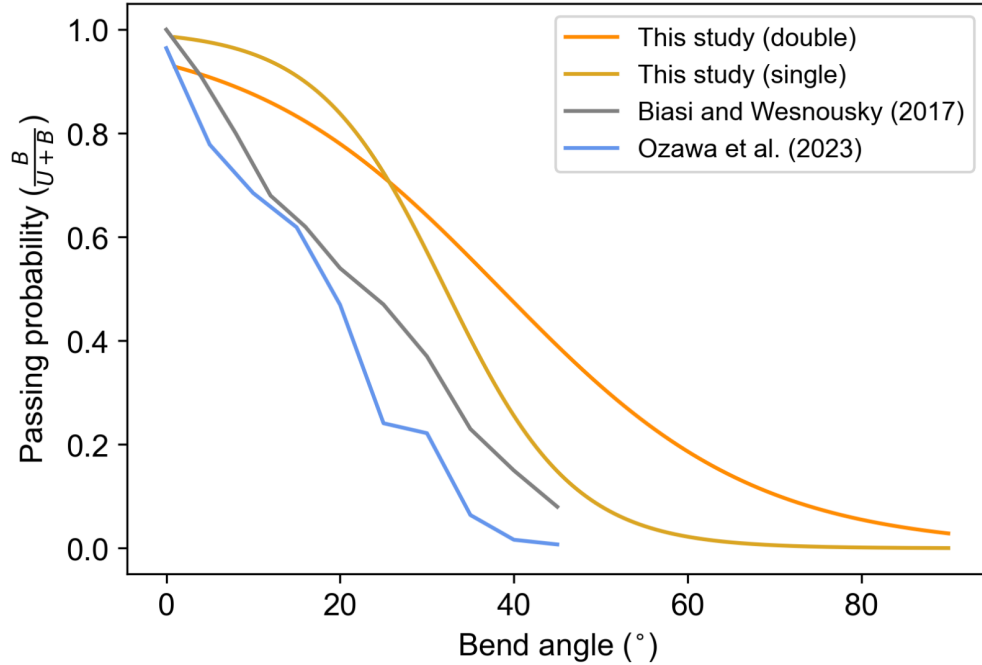
149 **Figure S2.** Logistic regressions (gray) showing the passing probabilities of restraining and
 150 releasing step-overs and double bends. The data are shown as beehive plots, which show all data
 151 points in each classification, breached in teal and unbreached in orange. The ROC score for each
 152 logistic regression is shown on the top right of each panel. Top and bottom left: Passing probability
 153 as a function of step-over width. Top and bottom right: Passing probability as a function of double
 154 bend angle. The gray shading shows the 95% confidence intervals of the regressions calculated by
 155 bootstrapping.



156

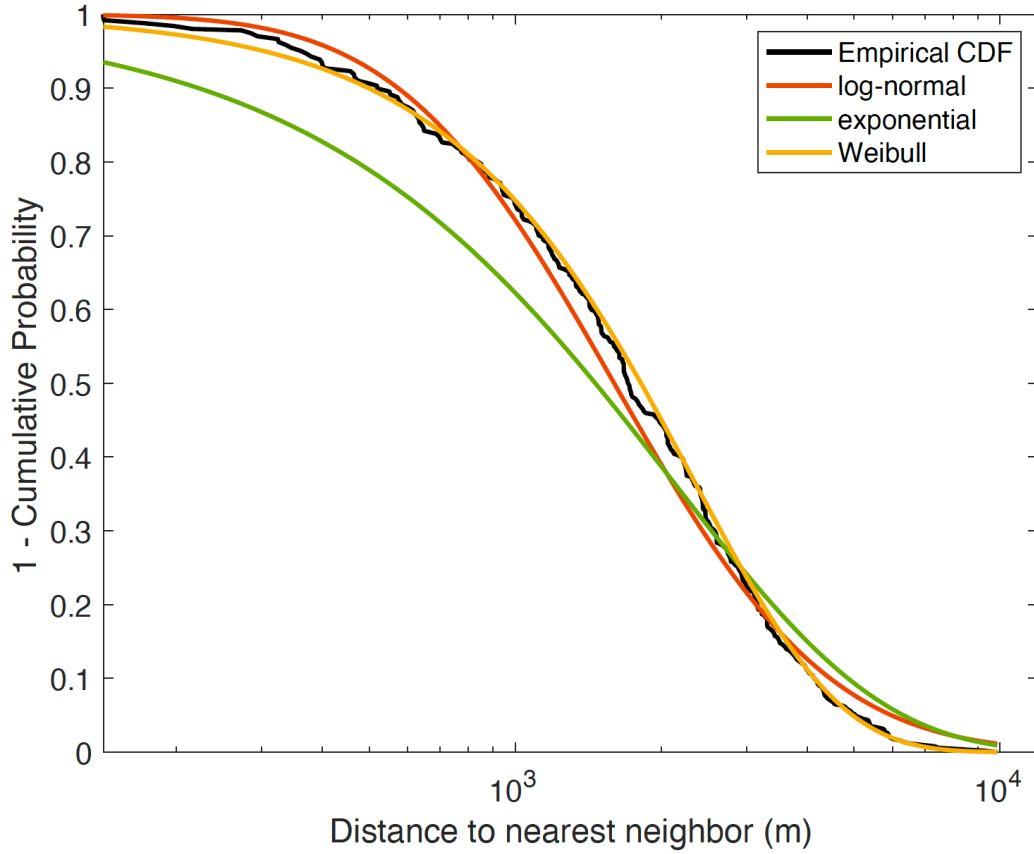
157 **Figure S3.** Confusion matrices for the logistic models for step-overs, single and double bends,
 158 and gaps in Figure 3. Darker colors in the matching diagonals indicate better diagnosis of the
 159 breached and unbreached features by the logistic fits.

160



161

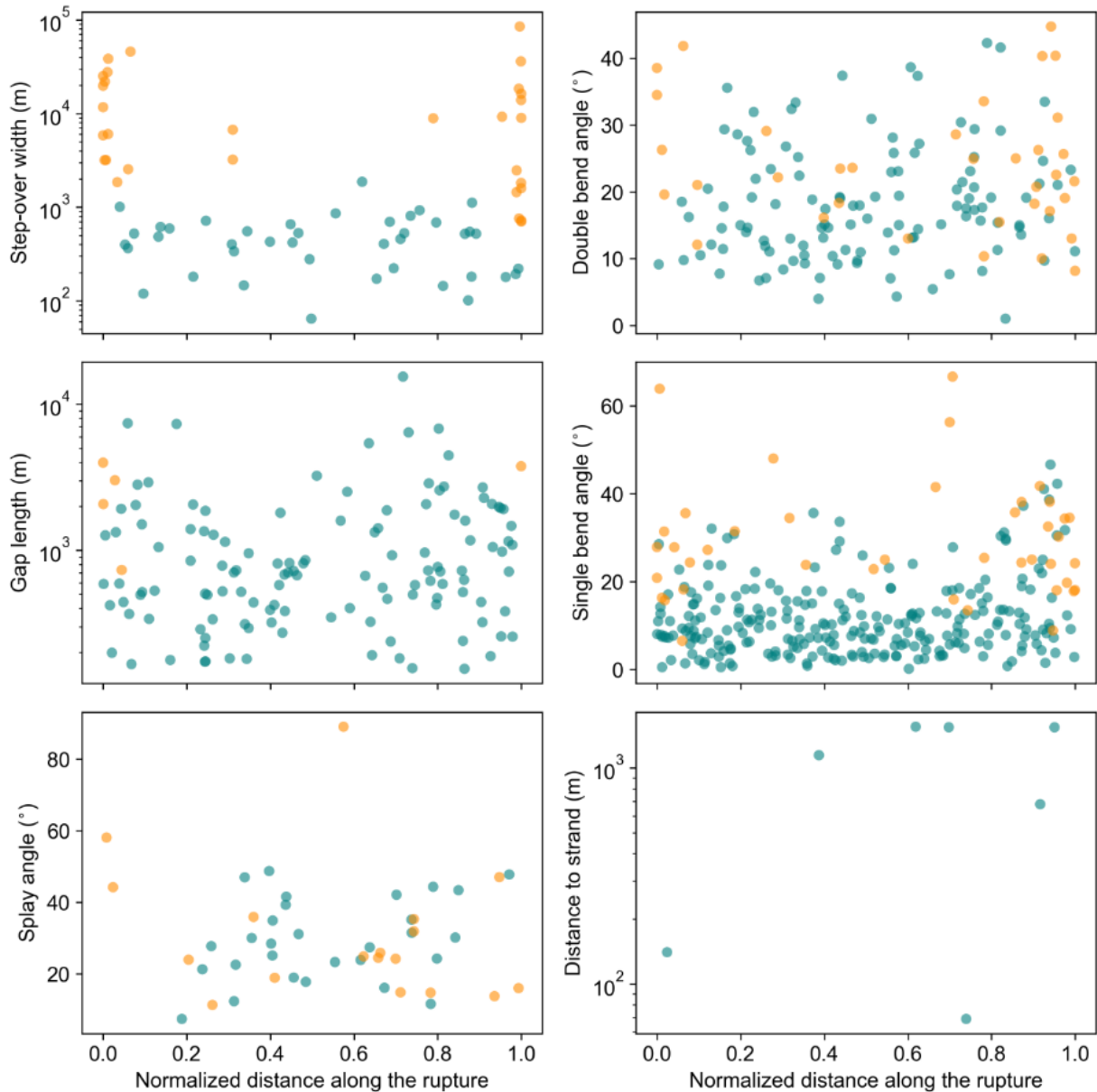
162 **Figure S4.** Comparison of the passing probabilities for different bend angles estimated in Biasi
 163 and Wesnousky (2017), Ozawa et al. (2023), and this study. Passing probability estimated as the
 164 number of breached bends per bin over the total number of bends in that bin in previous studies
 165 and with logistic regressions here. Note that the Biasi and Wesnousky (2017) passing probabilities
 166 include both single and double bends without discriminating between them, and the Ozawa et al.
 167 (2023) passing probabilities only include double bends.



168

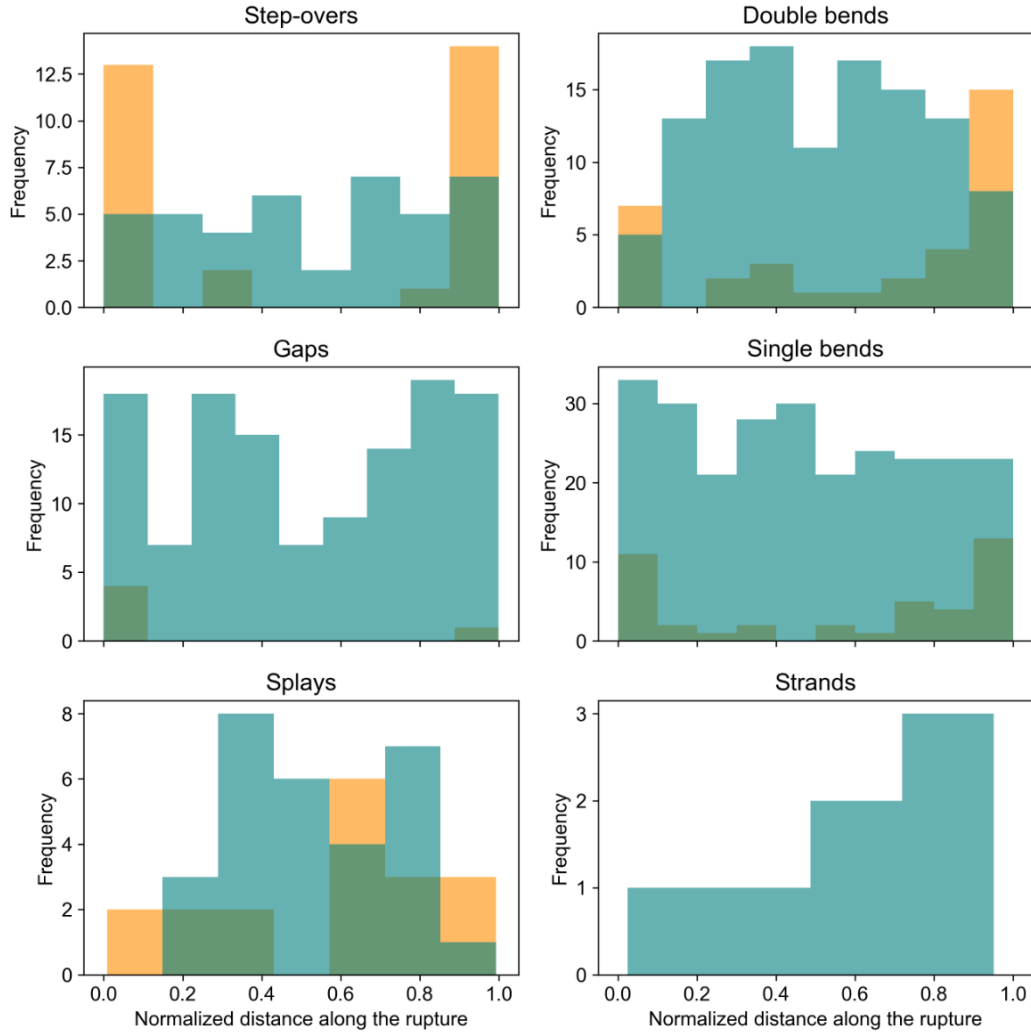
169 **Figure S5.** Empirical complementary cumulative distribution function of the distances to nearest
 170 neighbor for all breached earthquake gates. Complementary cumulative distribution functions for
 171 a log-normal, an exponential, and a Weibull fit are shown in orange, green, and yellow,
 172 respectively.

173



174

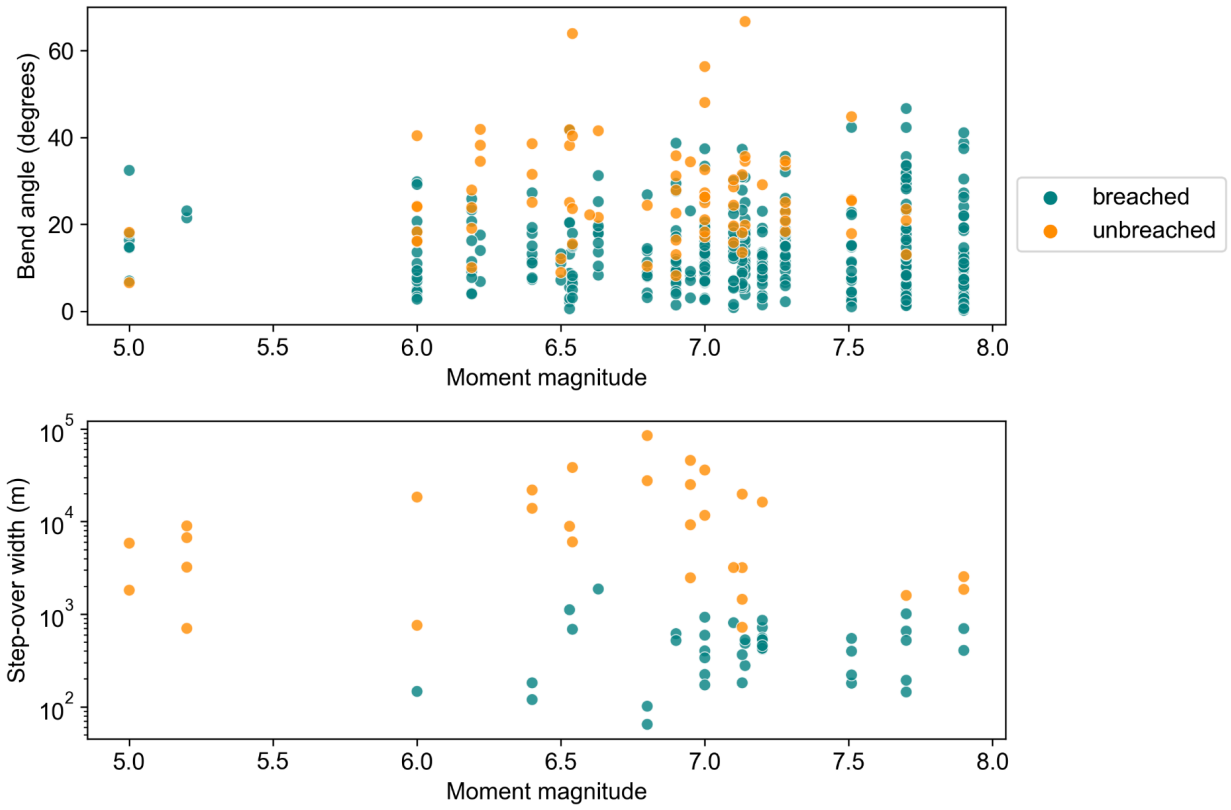
175 **Figure S6.** Distribution of breached (teal) and unbreached (orange) earthquake gates along the
 176 normalized surface rupture lengths of the 31 strike-slip events. The rupture lengths are based on
 177 the FDHI database event coordinate systems (ECS) reference lines (Sarmiento et al., 2021). There
 178 are some unbreached gates not at the edge of the ruptures. This is because, at some locations, there
 179 were two or more earthquake gates available, so that the gate the rupture continues past is mapped
 180 as breached and the remaining ones get mapped as unbreached (see methods for details).



181

182 **Figure S7.** Frequency of earthquake gates, breached and unbreached in teal and orange
 183 respectively, along the normalized surface rupture length for each earthquake gate type.
 184 Transparency is used to allow for visualization of the unbreached boxes (orange). Because we do
 185 not consider rupture propagation direction, as it is unknown for many of the events, the orientation
 186 of the x axis of this plot does not carry meaning.

187

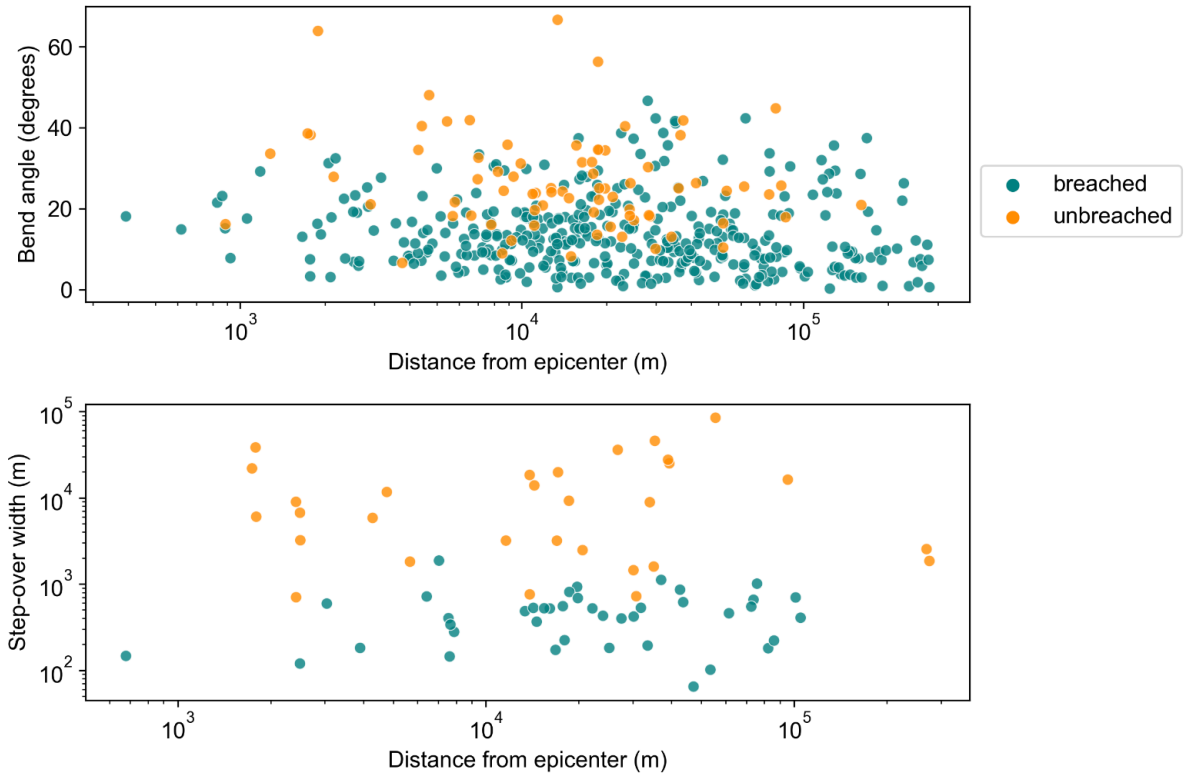


188

189 **Figure S8.** Bend angle (top) and step-over width (bottom) versus event moment magnitude for

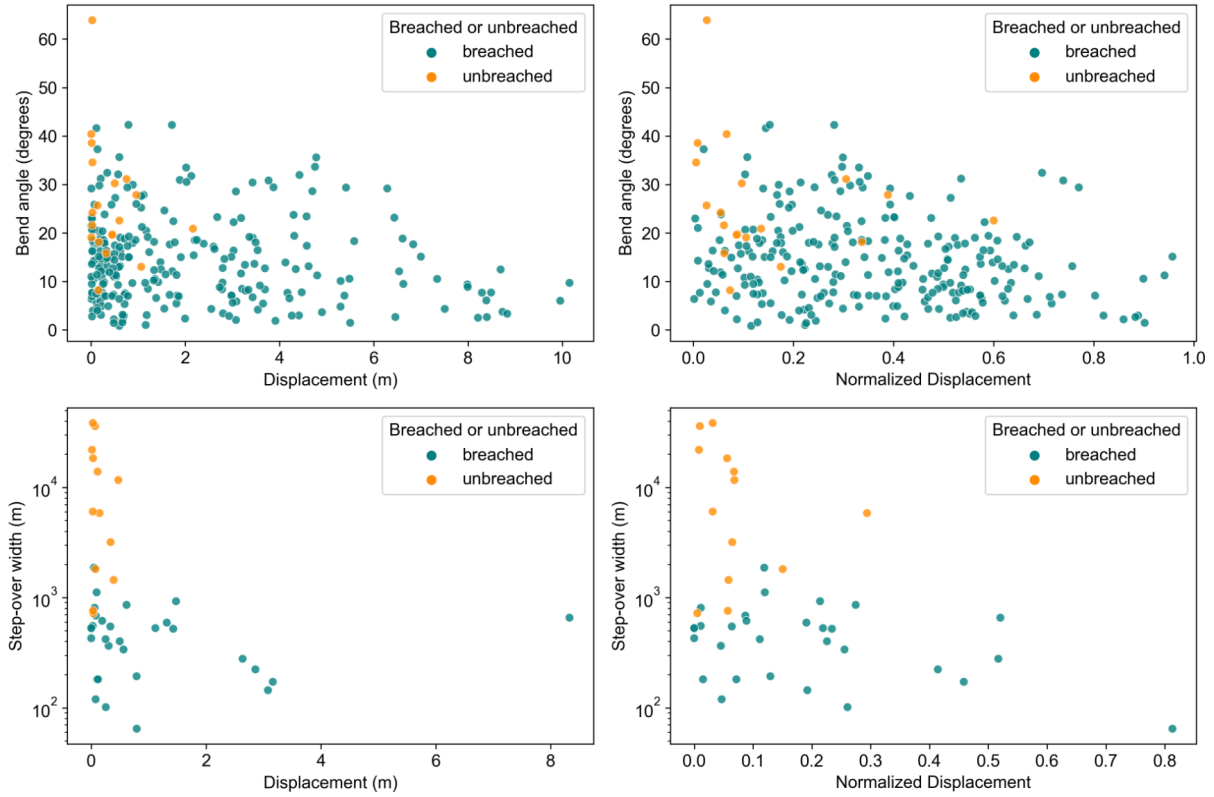
190 each of the events considered in this study.

191



192

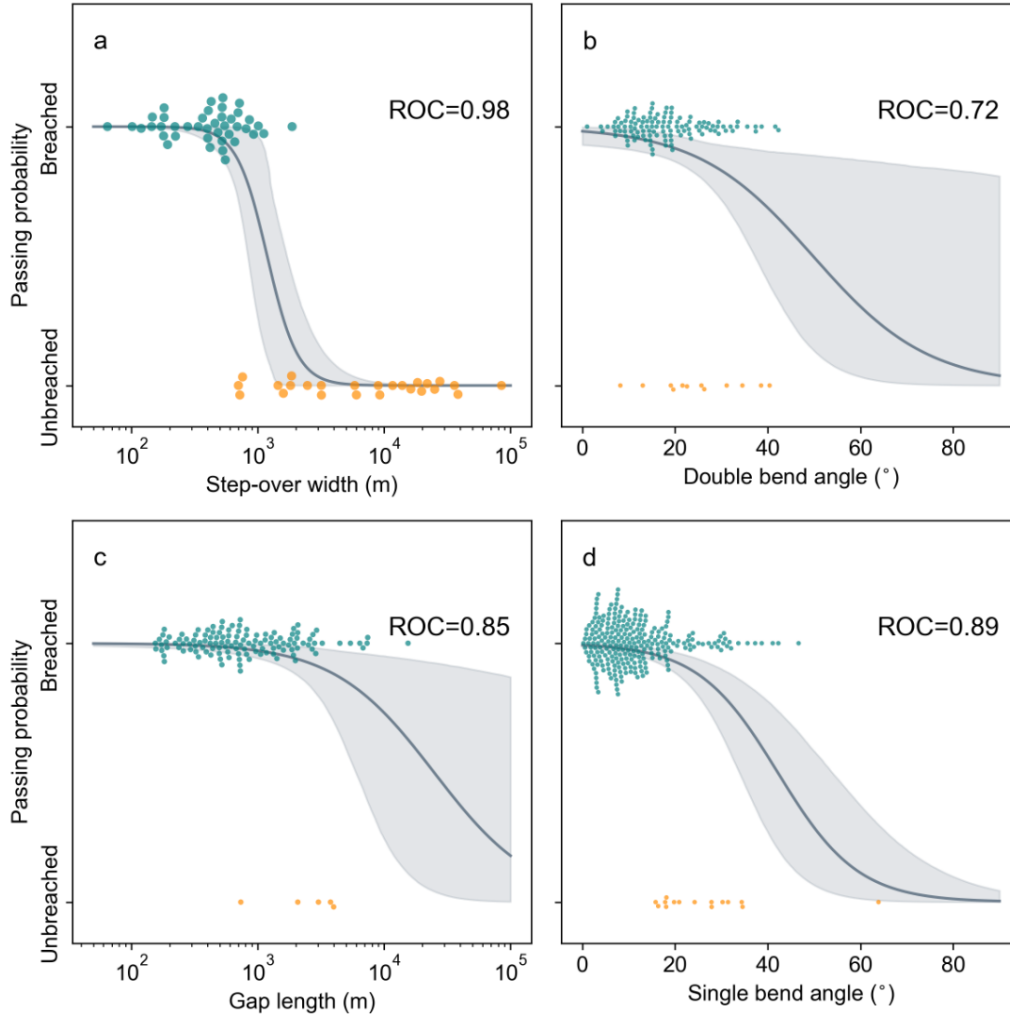
193 **Figure S9.** Gate size versus minimum distance to event epicenter. The event epicenters are sourced
194 from the FDHI database (Sarmiento et al. (2021)). Note some epicenters in the database are off-
195 fault.



196

197 **Figure S10.** Average slip at bends (top), including both single and double bends, and step-overs
 198 (bottom) as a function of bend angle and step-over width. The slip is computed as the average
 199 value for all slip measurements available within 500 meters of the earthquake gate. The plots on
 200 the left have the mean slip and the ones on the right have the mean slip normalized by the maximum
 201 slip of the event the gate was measured for.

202



203

204 **Figure S11.** Passing probabilities as a function of geometry including only unbreached earthquake

205 gates at rupture termini (within 5% of the rupture length of each termini). All breached gates are

206 included.

207

Reference Fault Map	Location	References
Quaternary Fault and Fold Database of the United States	United States	USGS and CGS
New Zealand Active Faults Database (NZAFD)	New Zealand	Langridge et al. (2016)
The Active Faults of Eurasia Database (AFEAD)	Europe and Asia	Bachmanov et al. (2021)
GEM Global Active Faults Database	Central and South America	Styron and Pagani (2020)

208

209 **Table S1.** Reference maps of active faults to measure unbreached feature characteristics with

210 respect to.

Table S2: Number of mapped features

Feature	Number mapped
Step-overs	71
Releasing step-overs	26
Restraining step-overs	45
Bends	449
Single bends	297
Double bends	152
Releasing double bends	80
Restraining double bends	72
Gaps	130
Splays	47
Strands	7

Table S3: p-values from the ks tests

Feature A	Feature B	p-value from ks test
Breached double bend	Unbreached double bend	5.049231e-03
Breached single bend	Unbreached single bend	2.679407e-17
Breached step-over	Unbreached step-over	2.340031e-14
Breached gaps	Unbreached gaps	1.418856e-02
Breached splay	Unbreached splay	6.938317e-01
Releasing unbreached bend	Restraining unbreached bend	7.370006e-01
Releasing breached bend	Restraining breached bend	1.402596e-01
Releasing breached step-over	Restraining breached step-over	4.827584e-01
Releasing unbreached step-over	Restraining unbreached step-over	6.820546e-01

Table S4: Passing probabilities from the logistic regressions

Feature	Closest geometry to passing probability = 50%	Units
Double bends	38	degrees
Single bends	32	degrees
Step-overs	1170	meters
Gaps	24500	meters

Table S5: Passing probability on straight section

Feature	Passing probability per meter	Stopping probability per meter
Straight segment	0.99999	0.00001

Event	Termini on straight segments/Total termini	Features at termini
1. Parkfield 1966	1/2	Bend
2. Izmit-Kocaeli	1/2	Bend
3. Landers	4/6	Bends
4. Hector Mine	0/3	Bends, step-overs, gap
5. Balochistan	1/2	Bend
6. Borrego	1/2	Bend
7. Imperial 1979	1/2	Bends, step-over
8. Superstition Hills	0/2	Step-overs, bends
9. Kobe	0/3	Bends
10. Denali	2/2	-
11. Duzce	0/2	Bends
12. Napa	0/3	Step-over, bends, gap
13. Yushu	0/2	Bends
14. Hualien	0/2	Bends
15. Darfield	0/2	Step-overs, bend
16. Galway Lake	0/2	Step-overs
17. Chalfant Valley	0/2	Bends
18. Zirkuh	1/2	Step-over
19. Ridgecrest (foreshock)	0/2	Step-overs, bend
20. Kumamoto	1/3	Bends
21. Ridgecrest (mainshock)	0/2	Step-over, bends
22. Imperial 1940	0/2	Step-overs, bends
23. San Miguel	0/2	Step-overs, bend
24. Yutian	1/2	Bend
25. Luzon	0/2	Bends, step-over, gap
26. Elmore Ranch	0/2	Bends
27. Pisayambo	0/2	Step-overs, bends
28. Izu Peninsula	0/2	Bends
29. Izu Oshima	1/2	Bend
30. Neftegorsk	0/2	Bends
31. Parkfield 2004	1/2	Bend
All events	16/70	-

Table 1: *

Table S6: Number of termini on straight fault segments and on earthquake gates for the events on the FDHI database.

Earthquake gate types

-  steptover breached
-  steptover unbreached
-  bend breached
-  bend unbreached
-  strand breached
-  splay breached
-  splay unbreached
-  gap breached
-  gap unbreached

Figure S13. Event: Parkfield1966 M_W 6.19 Date: '1966-06-28'

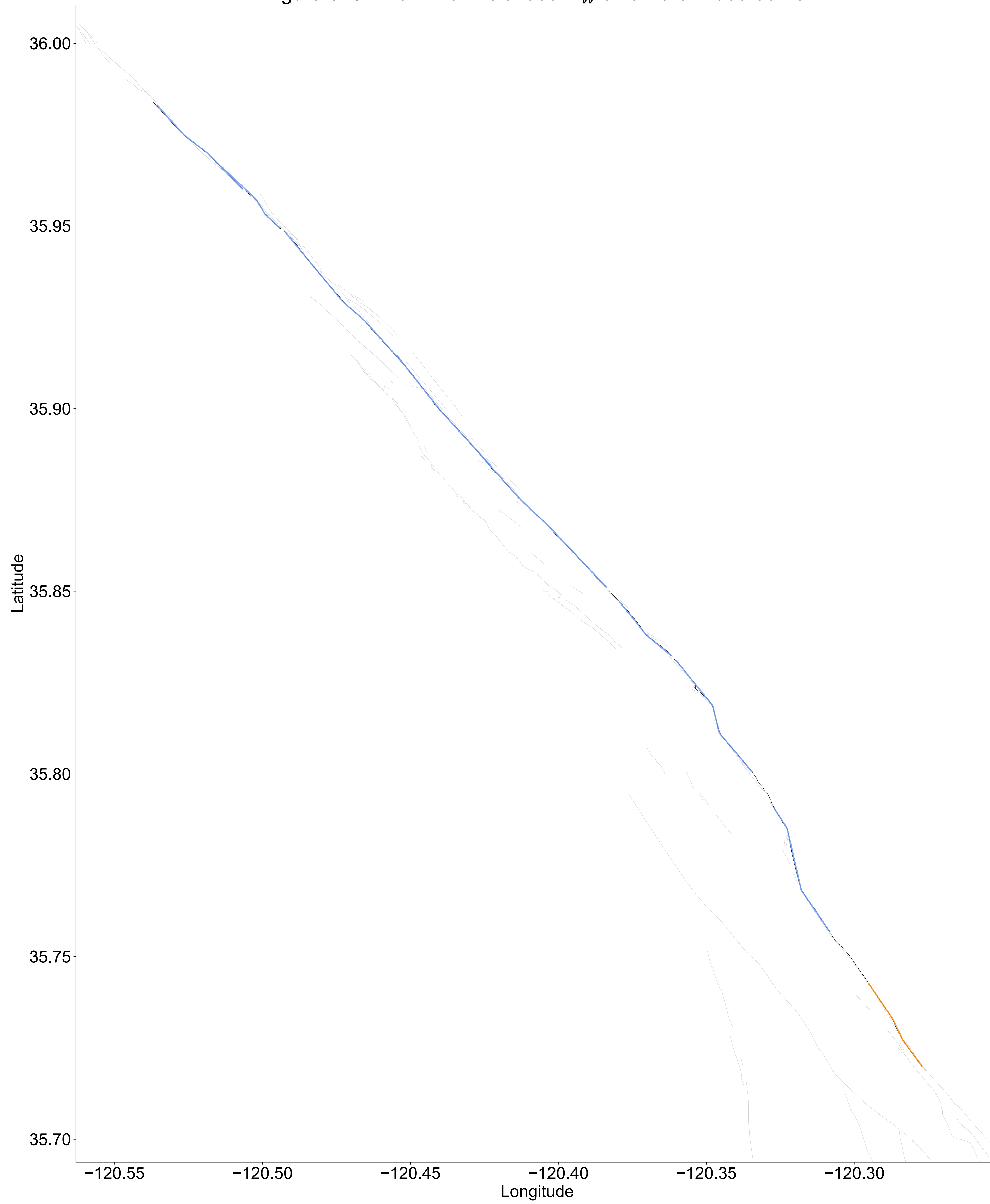


Figure S14. Event: HectorMine M_W 7.13 Date: '1999-10-16'

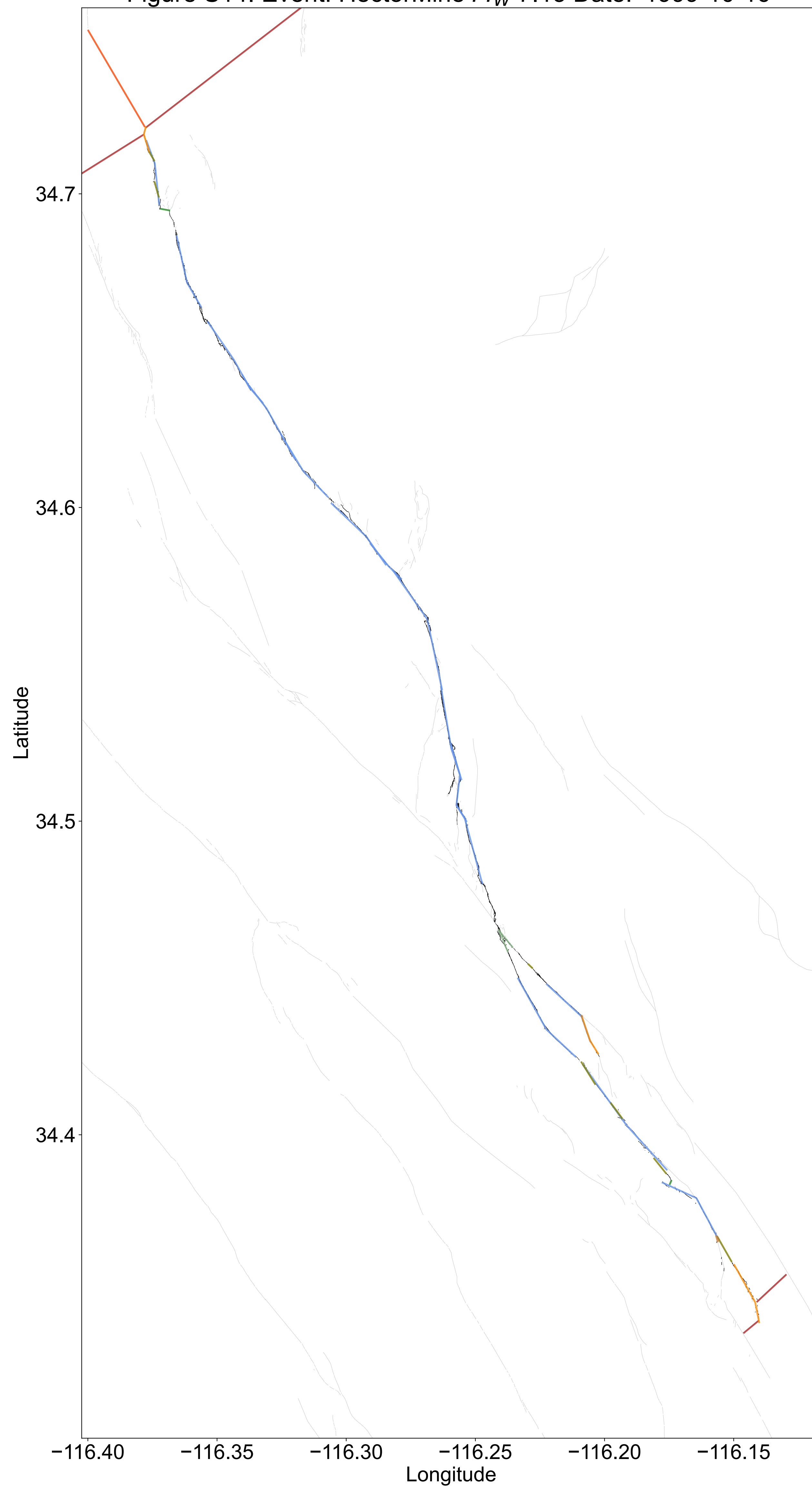


Figure S15. Event: Balochistan M_W 7.7 Date: '2013-09-24'

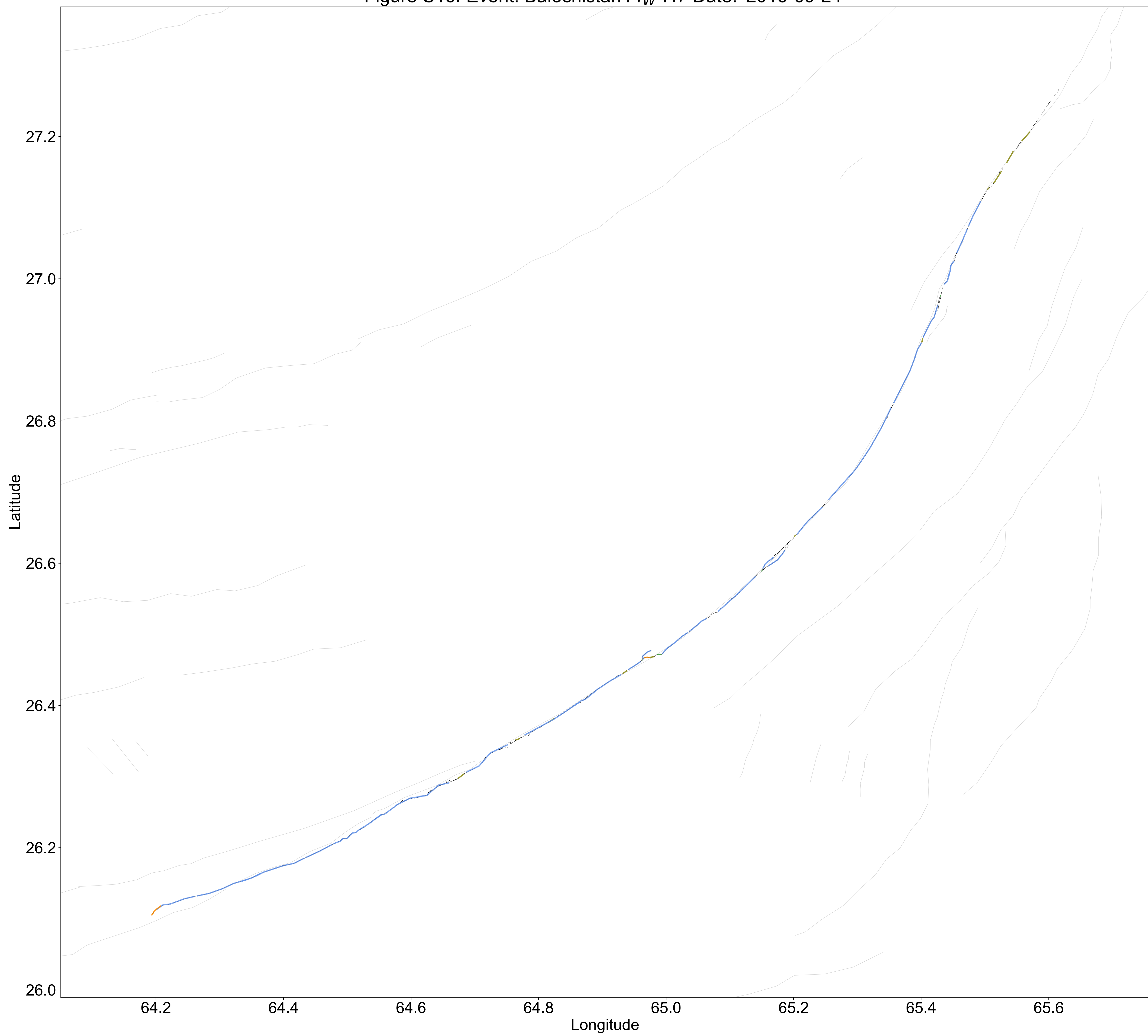


Figure S16. Event: Ridgecrest2 M_W 7.1 Date: '2019-07-06'

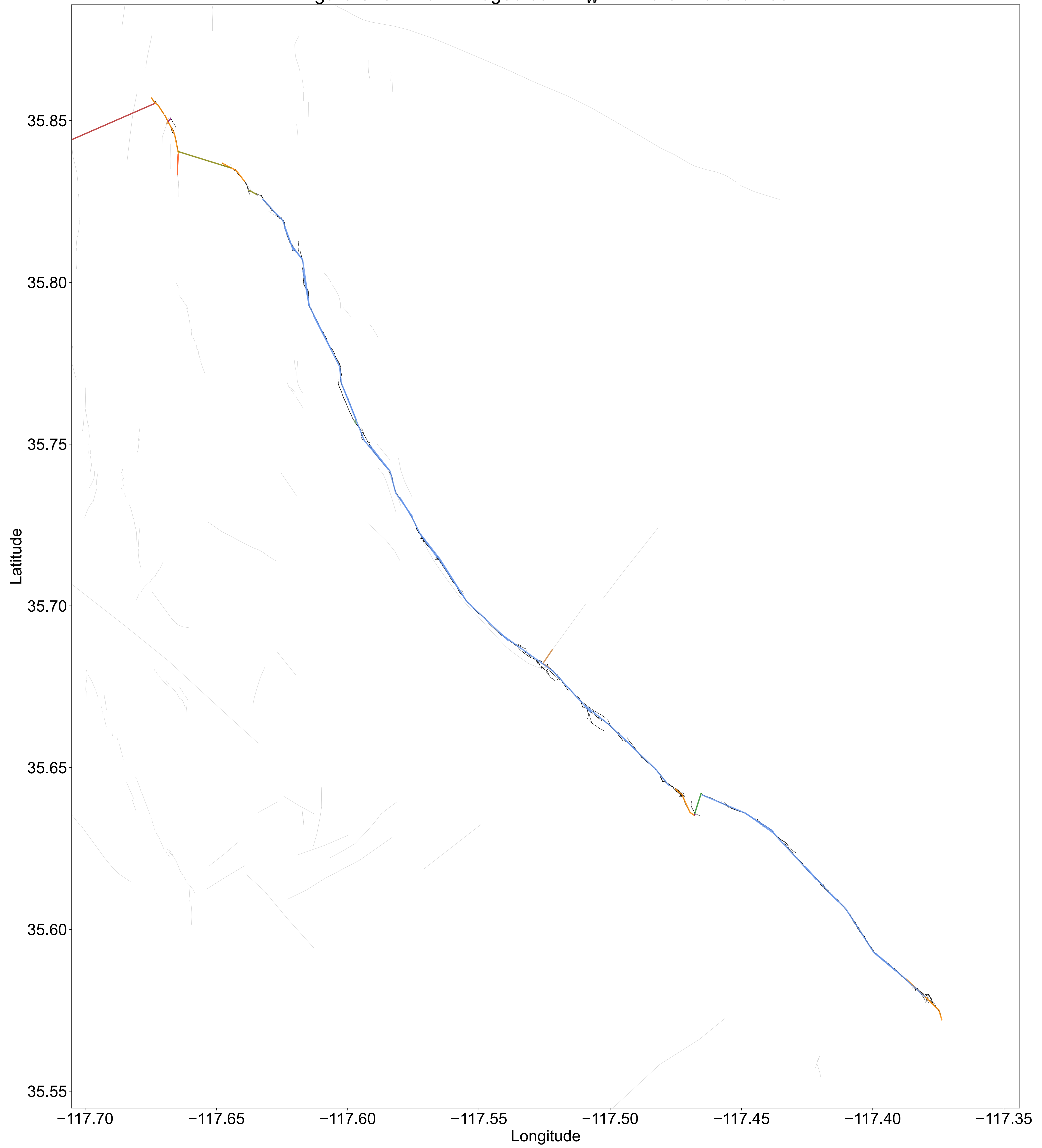


Figure S17. Event: Yutian M_W 6.9 Date: '2014-02-12'

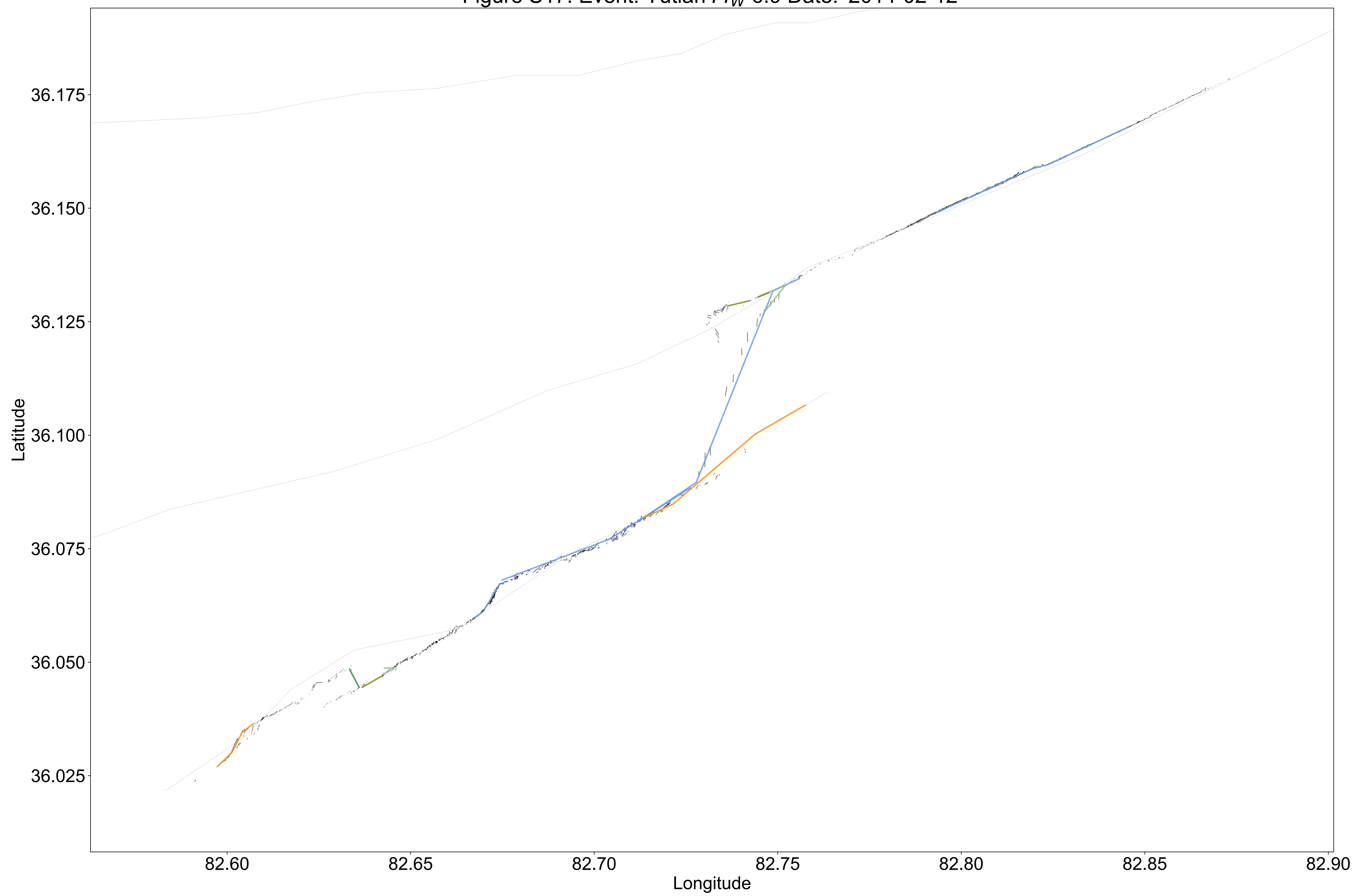


Figure S18. Event: Denali M_W 7.9 Date: '2002-11-03'

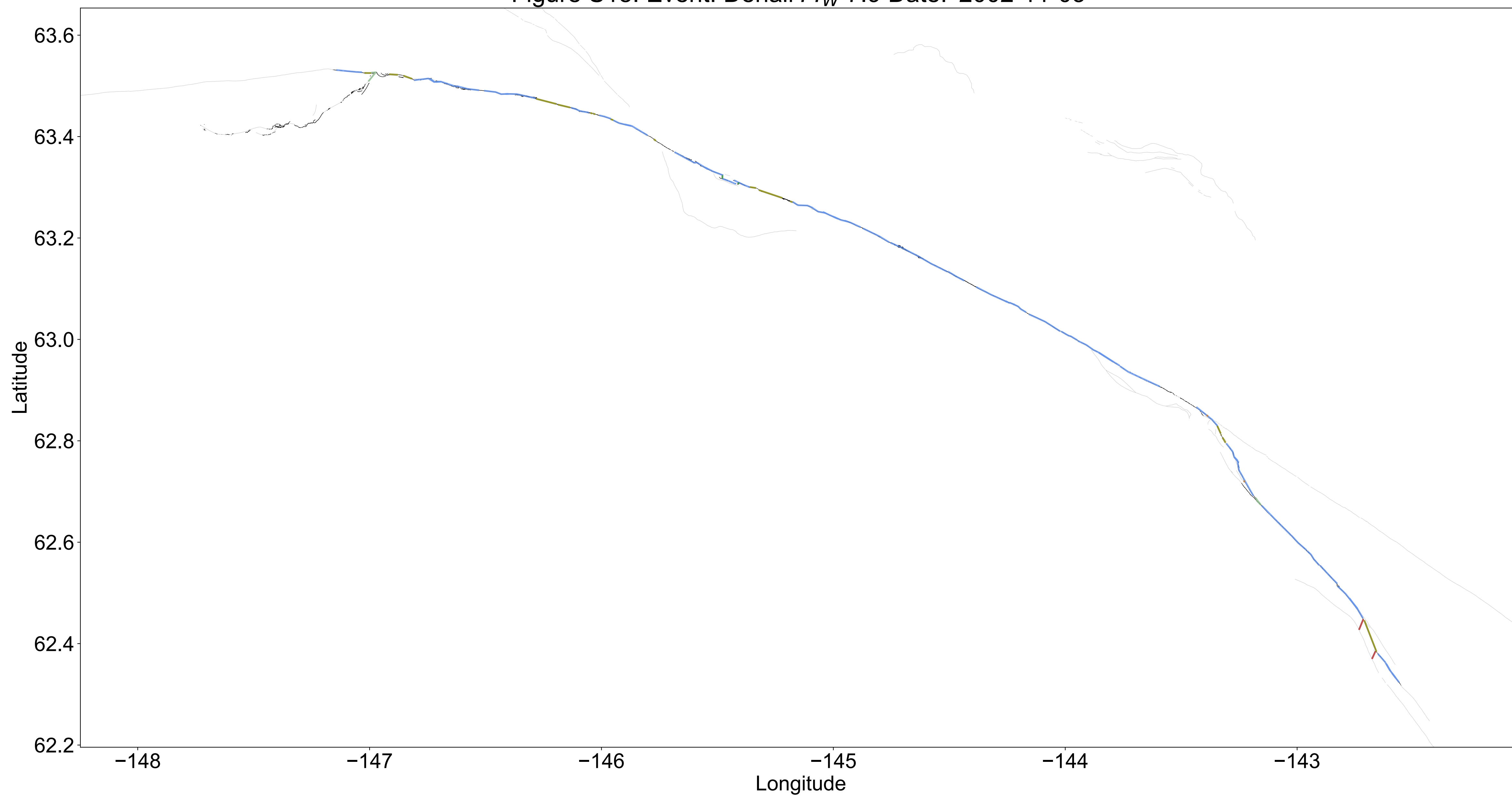


Figure S19. Event: ElmoreRanch M_W 6.22 Date: '1987-11-24'

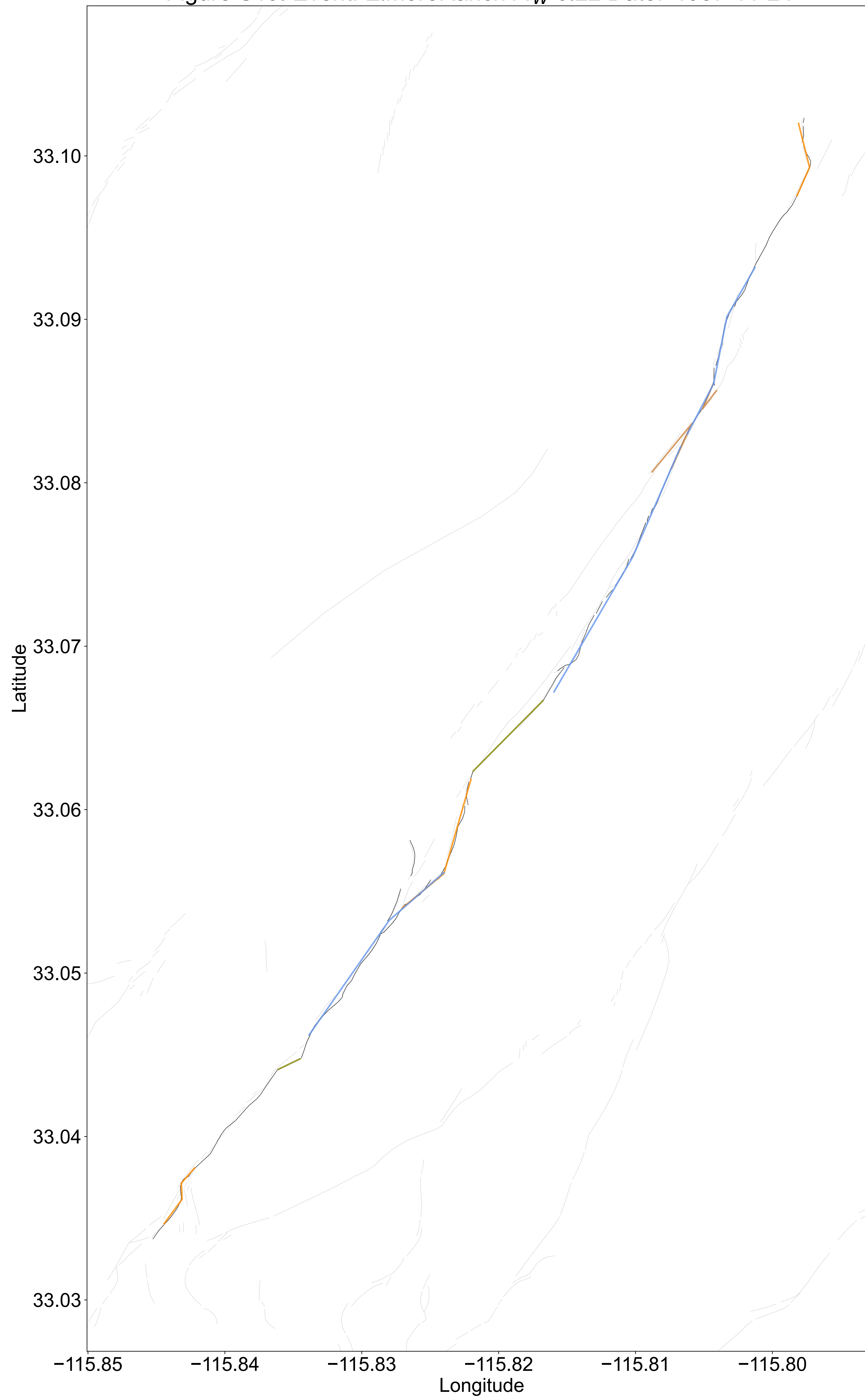


Figure S20. Event: IzuOshima M_W 6.6 Date: '1978-01-14'

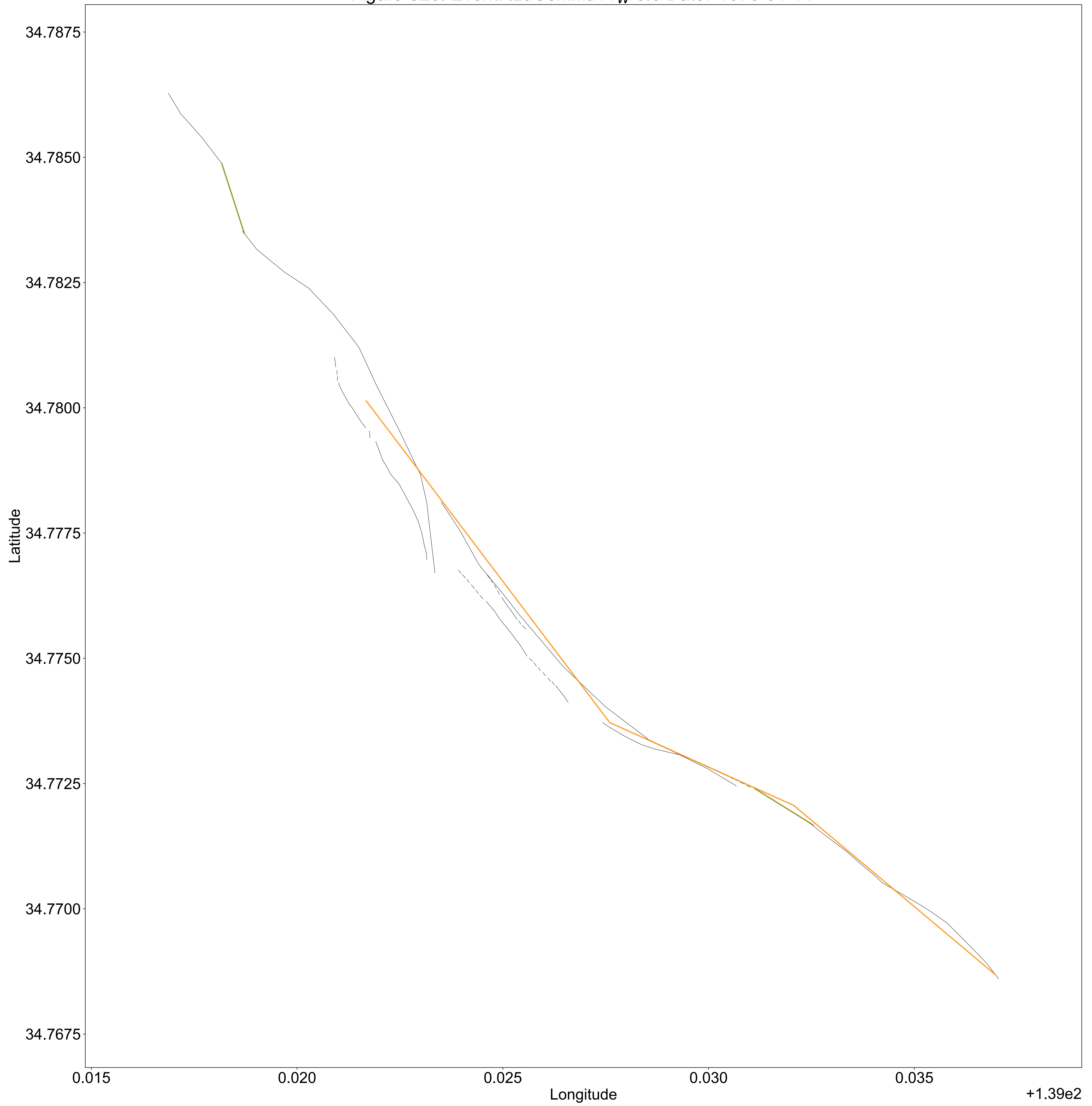


Figure S21. Event: Imperial1979 M_W 6.53 Date: '1979-10-15'

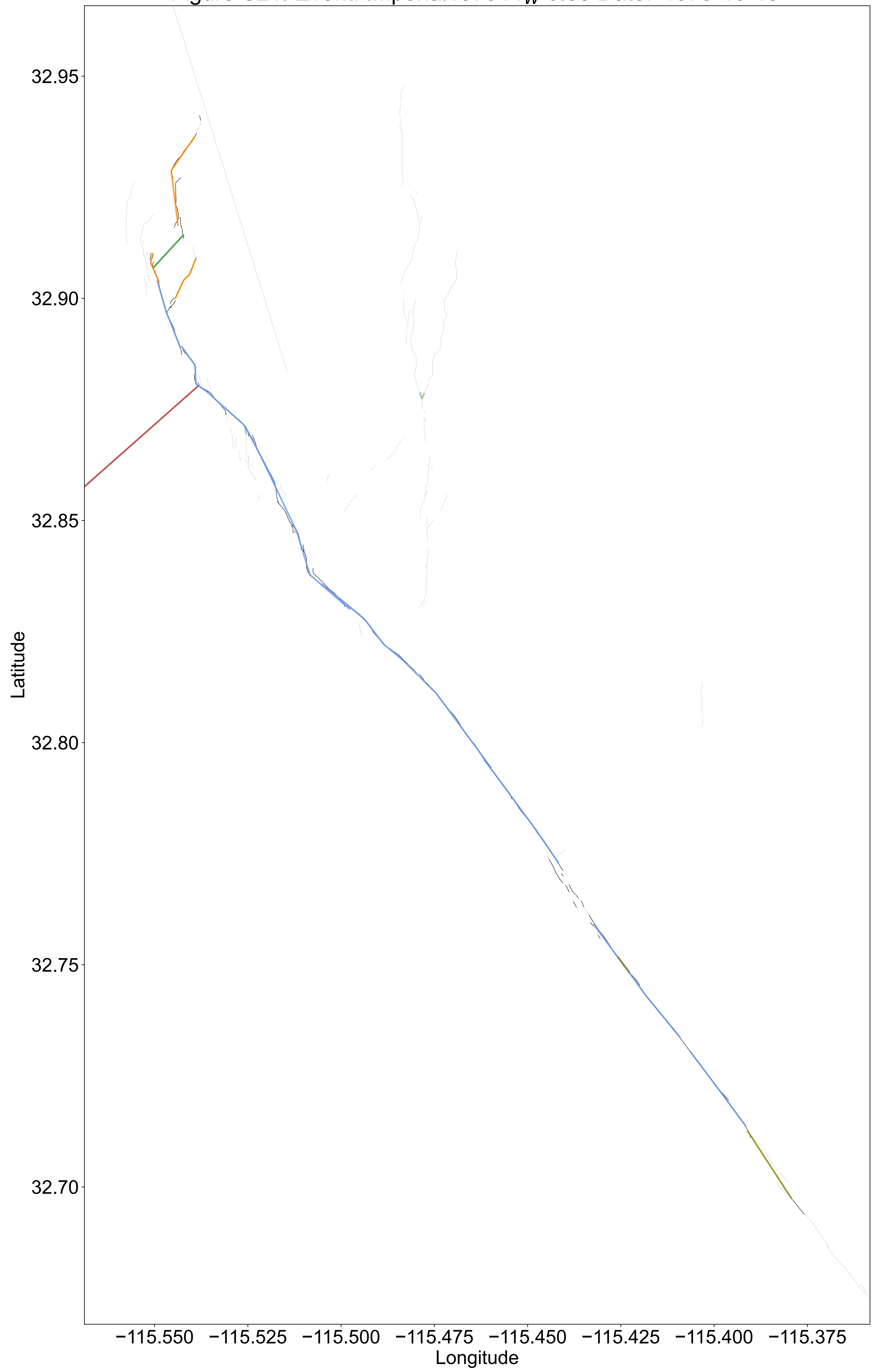


Figure S22. Event: Yushu M_W 6.9 Date: '2010-04-13'

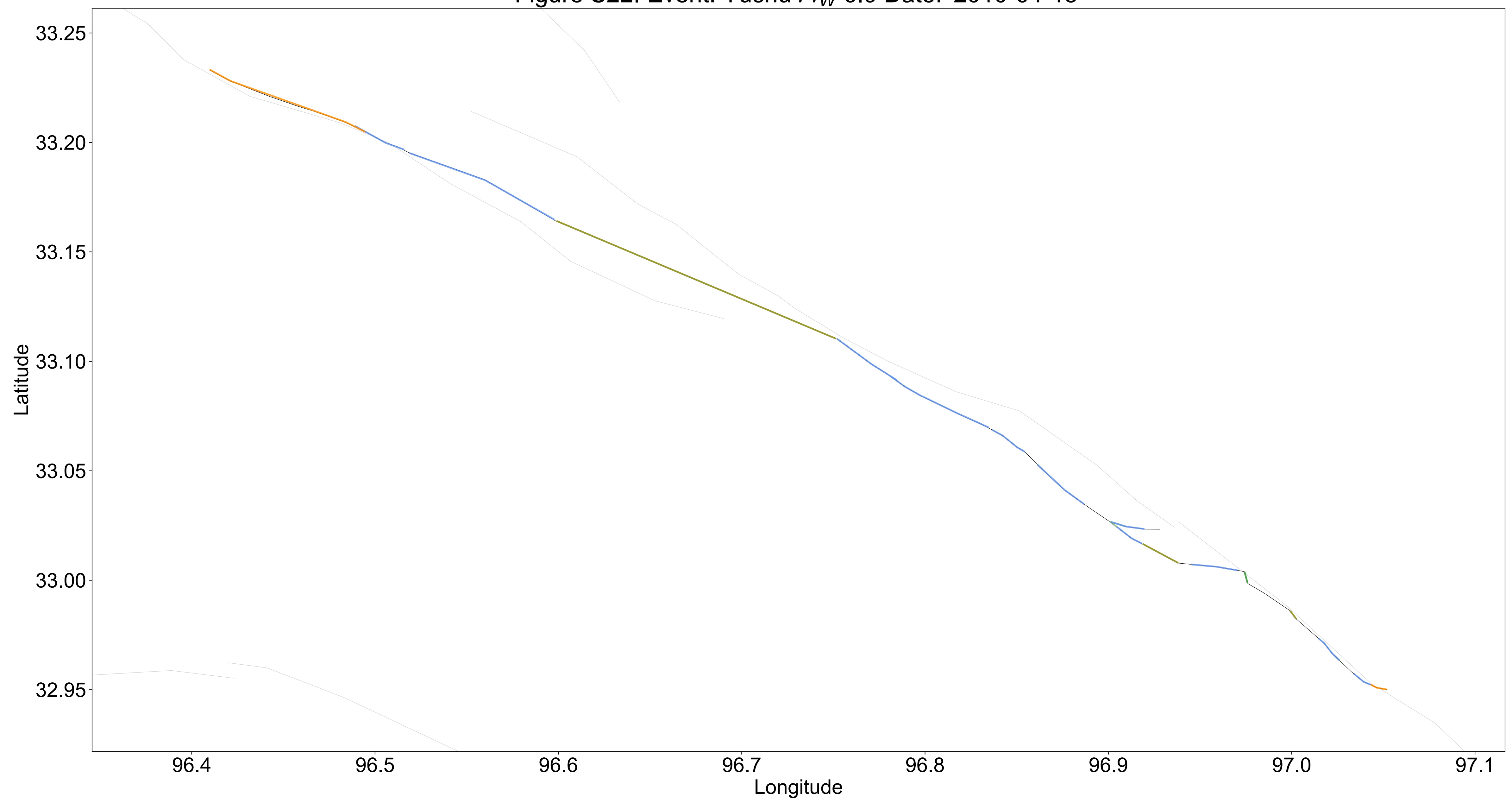


Figure S23. Event: Pisayambo M_W 5.0 Date: '2010-03-26'

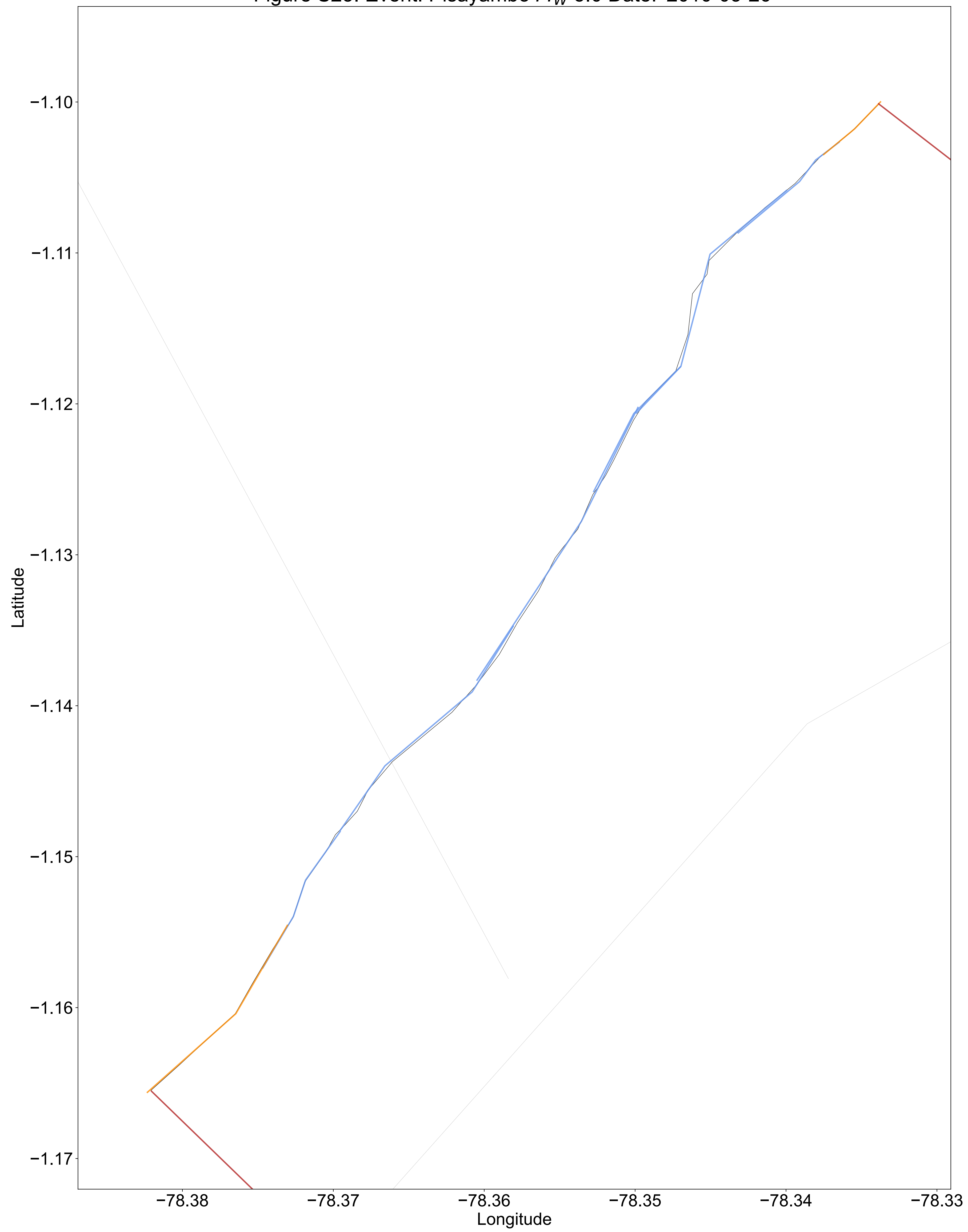


Figure S24. Event: Zirkuh M_W 7.2 Date: '1997-05-10'

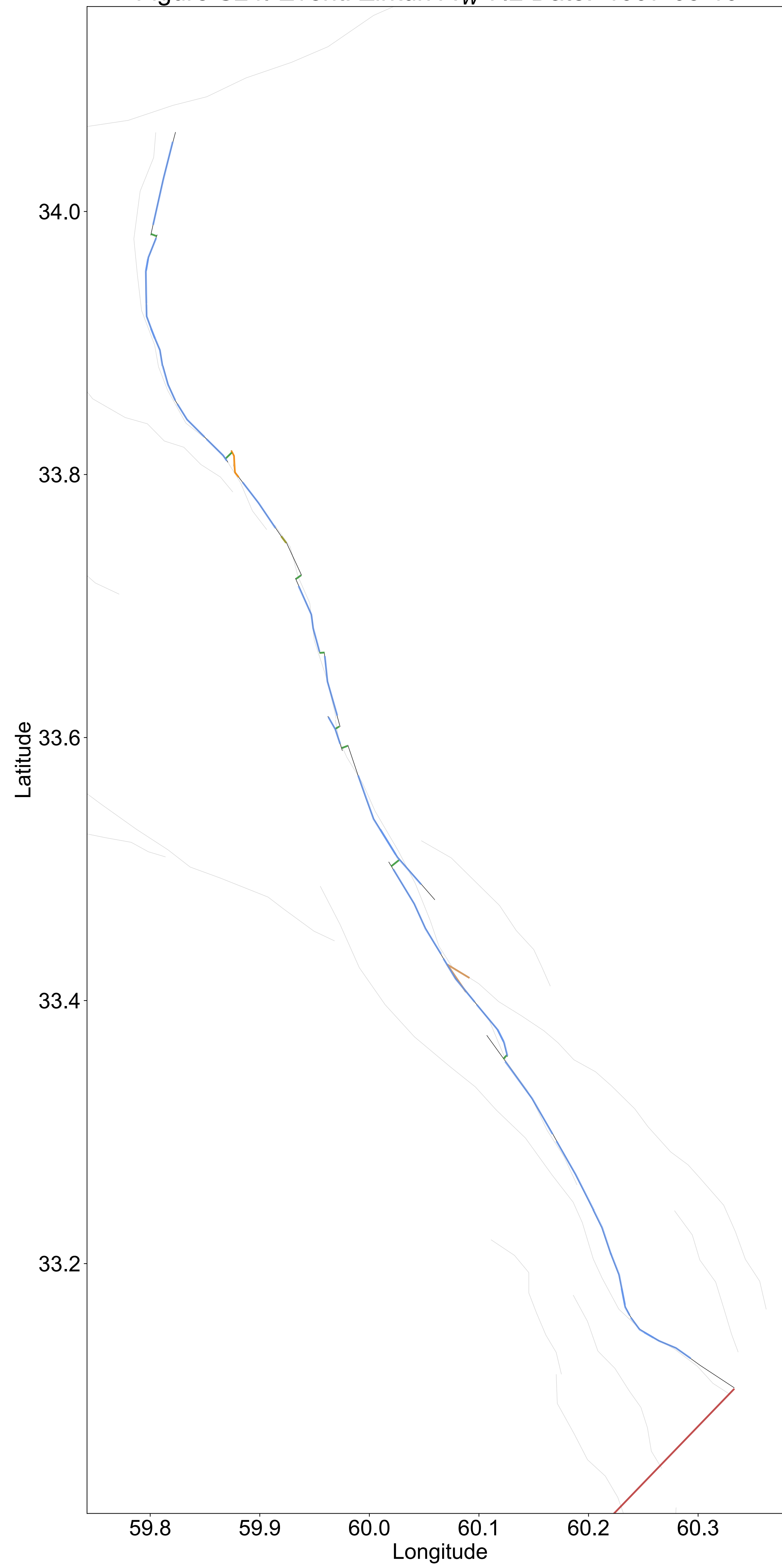


Figure S25. Event: Darfield M_W 7.0 Date: '2010-09-03'

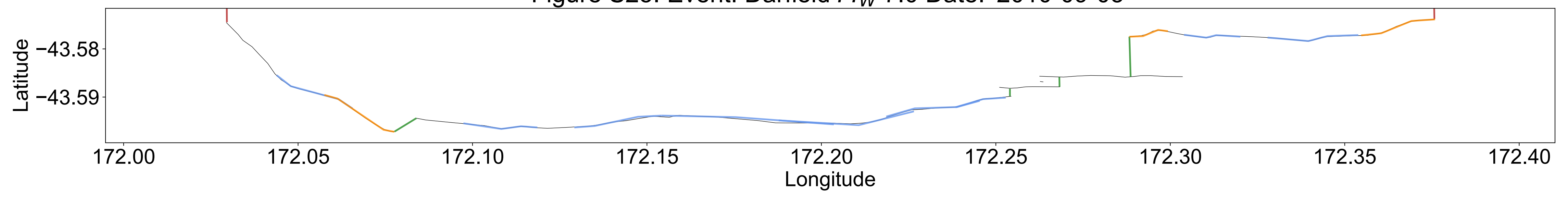


Figure S26. Event: Napa M_W 6.0 Date: '2014-08-24'

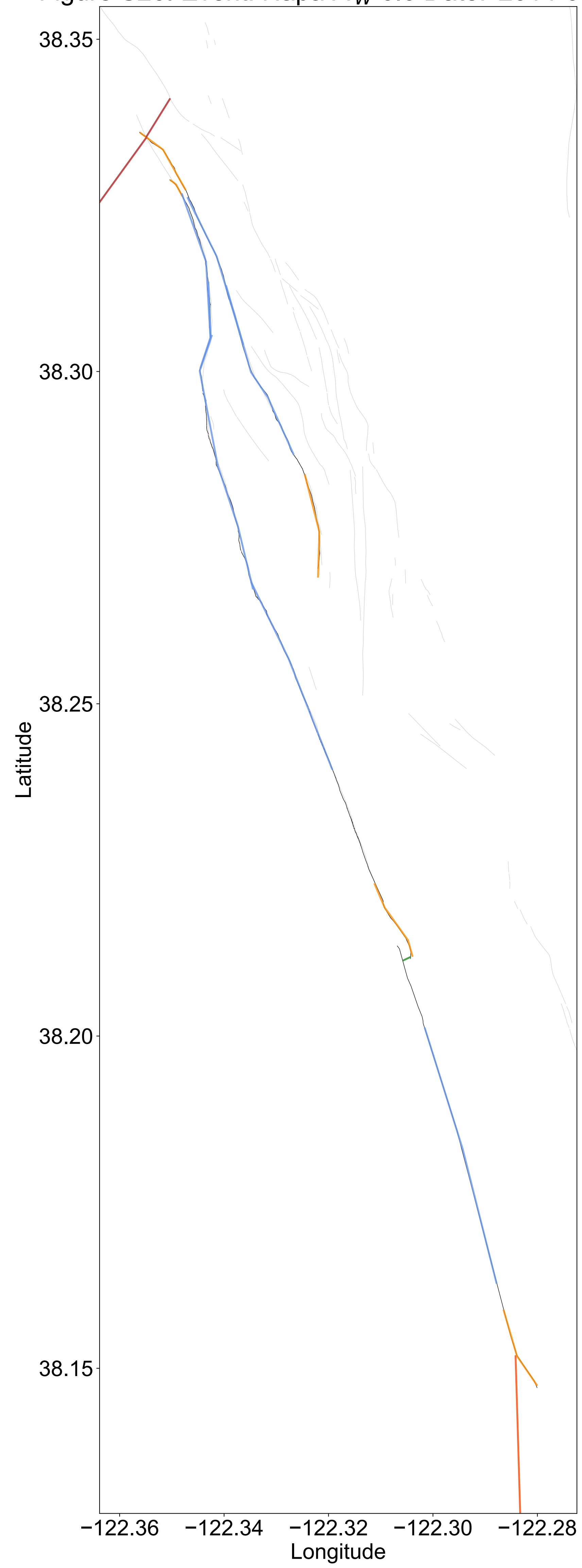


Figure S27. Event: Landers M_W 7.28 Date: '1992-06-28'

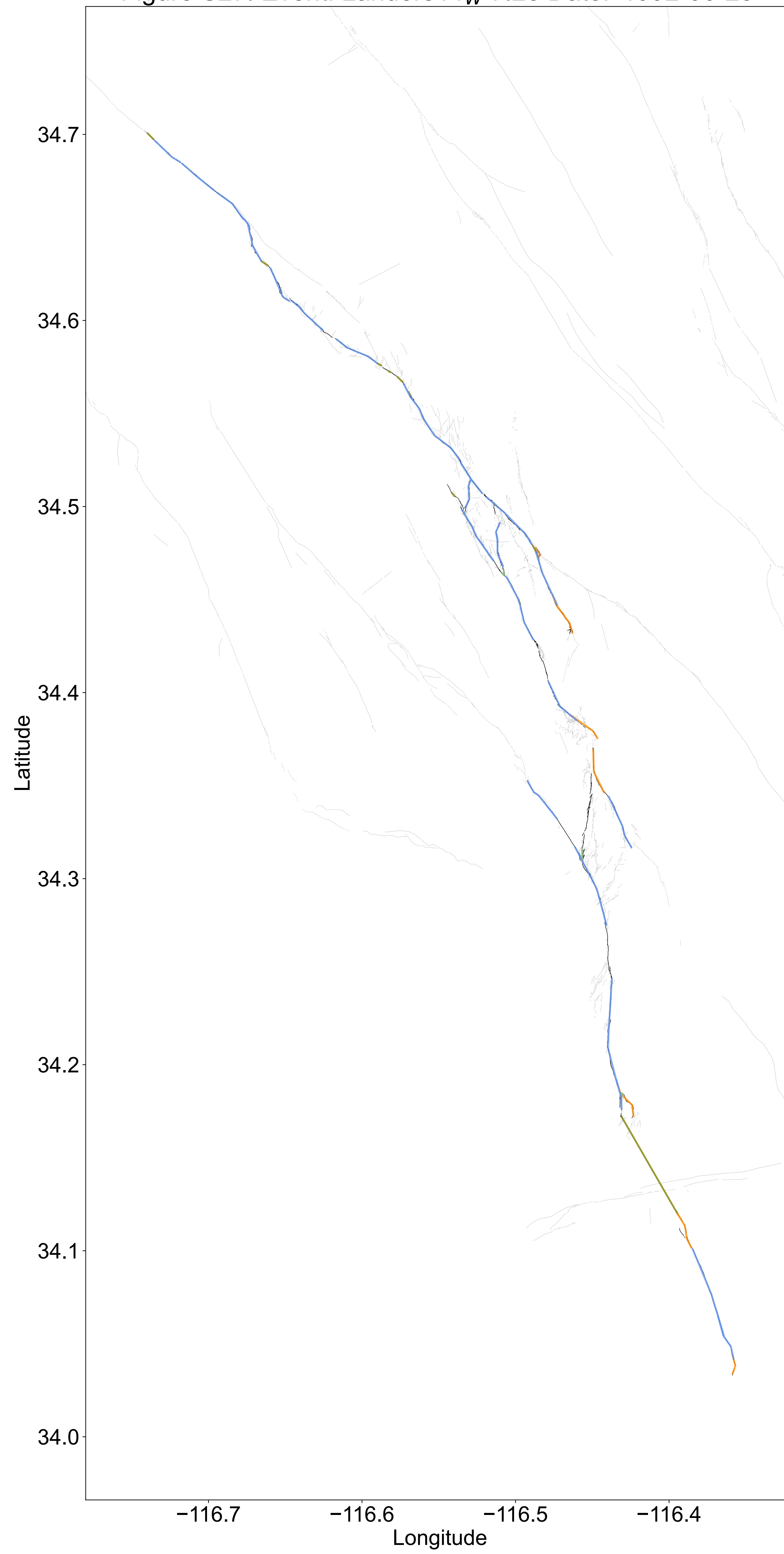


Figure S28. Event: SanMiguel M_W 6.8 Date: '1956-02-09'

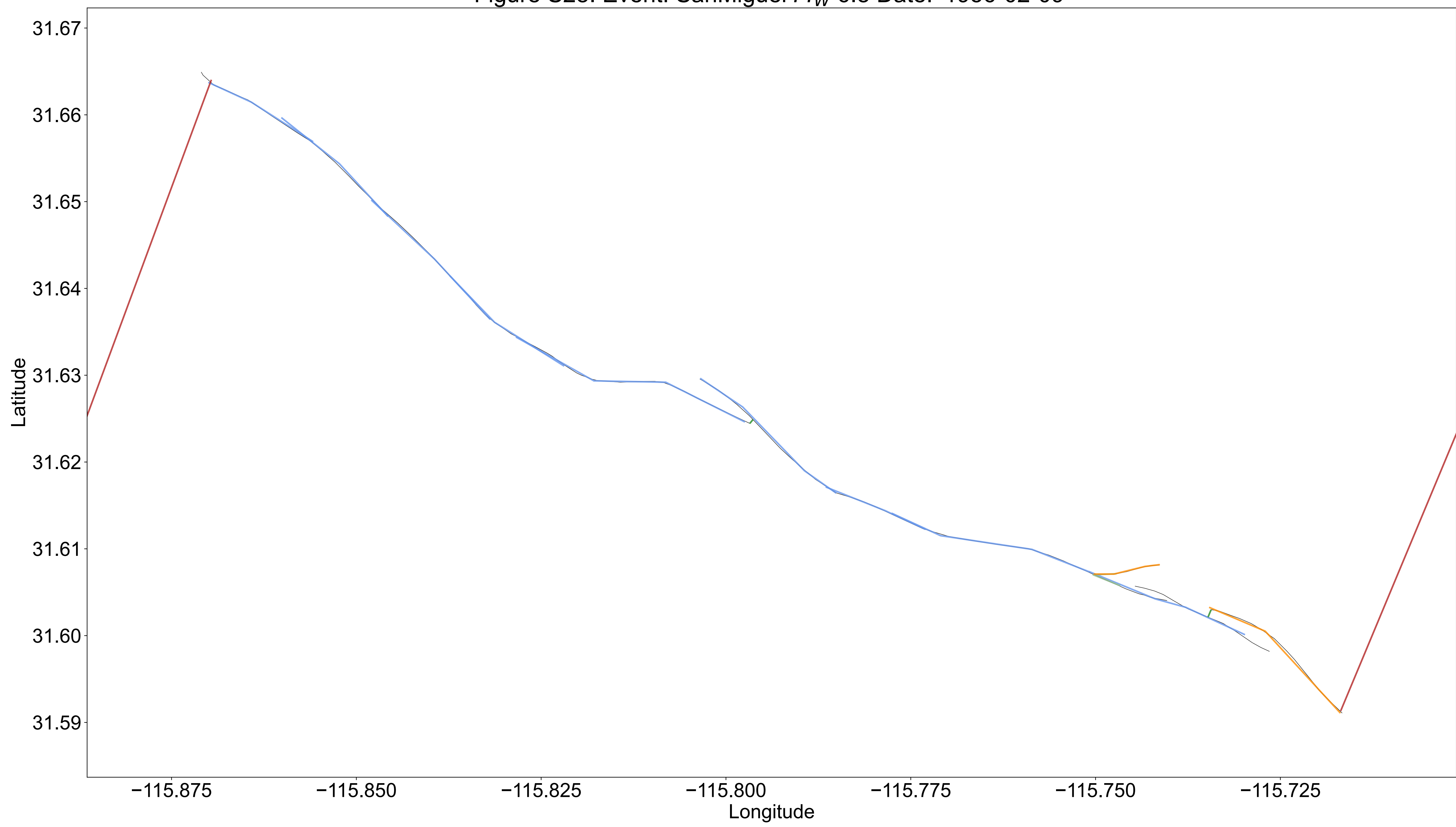


Figure S29. Event: ChalfantValley M_W 6.19 Date: '1986-07-21'

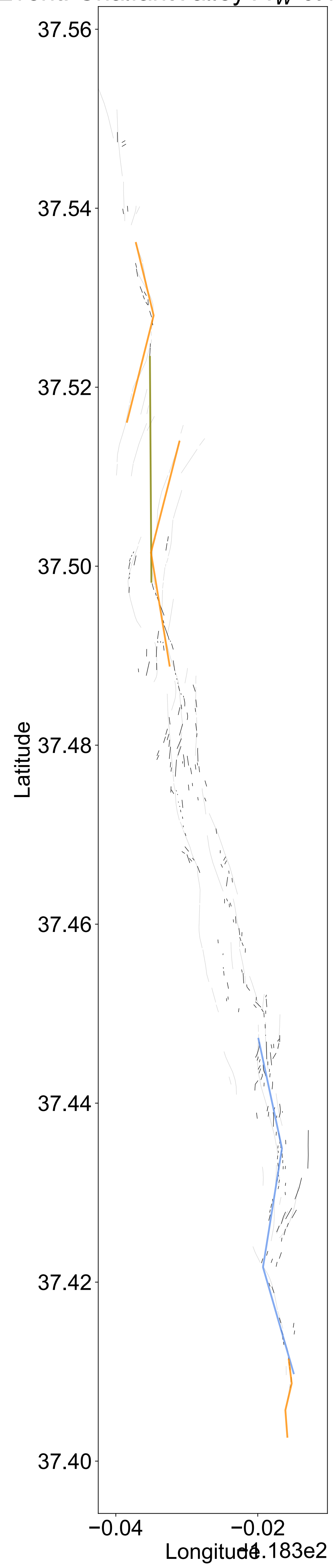


Figure S30. Event: Borrego M_W 6.63 Date: '1968-04-09'

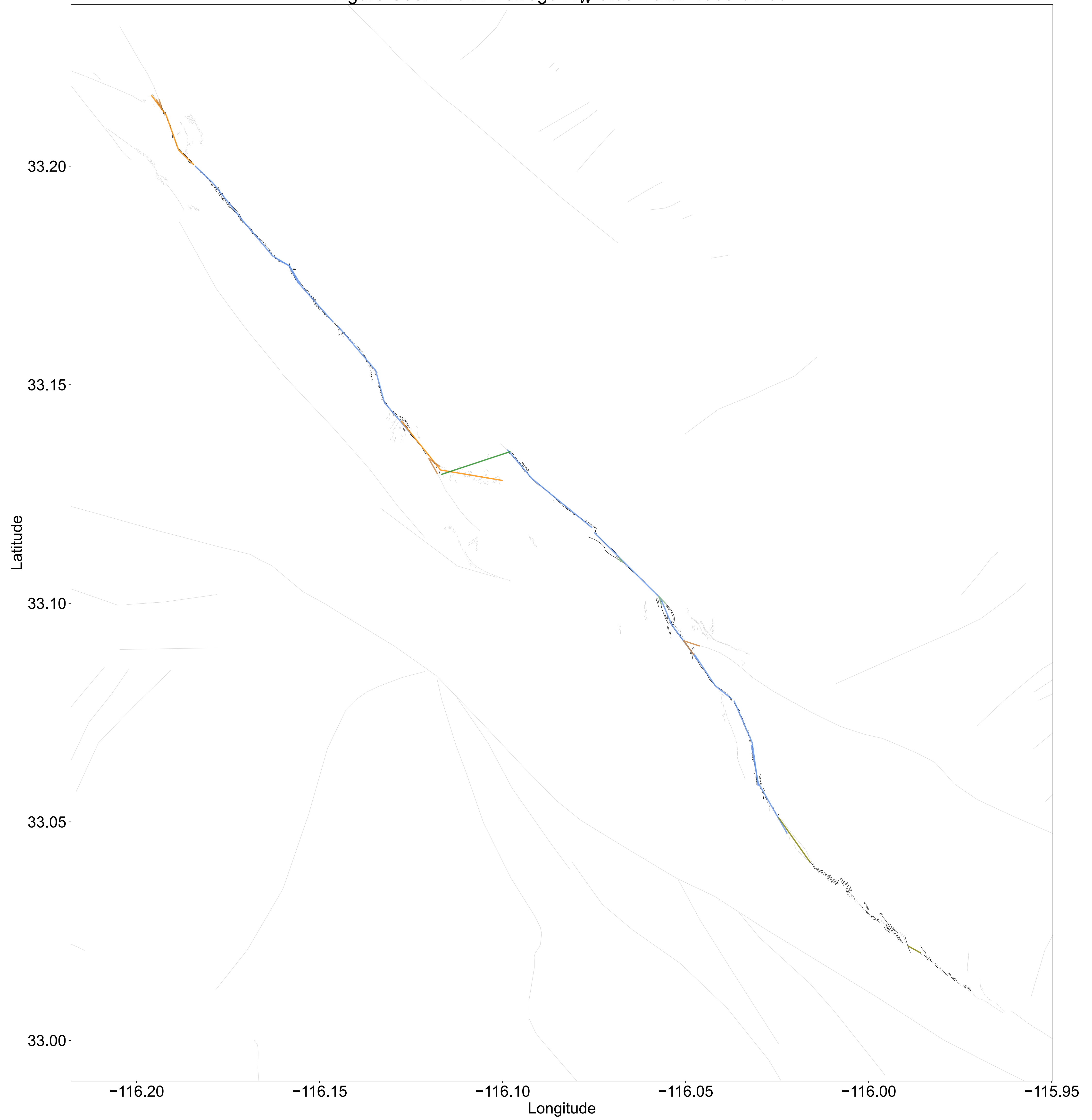


Figure S31. Event: Neftegorsk M_W 7.0 Date: '1995-05-27'

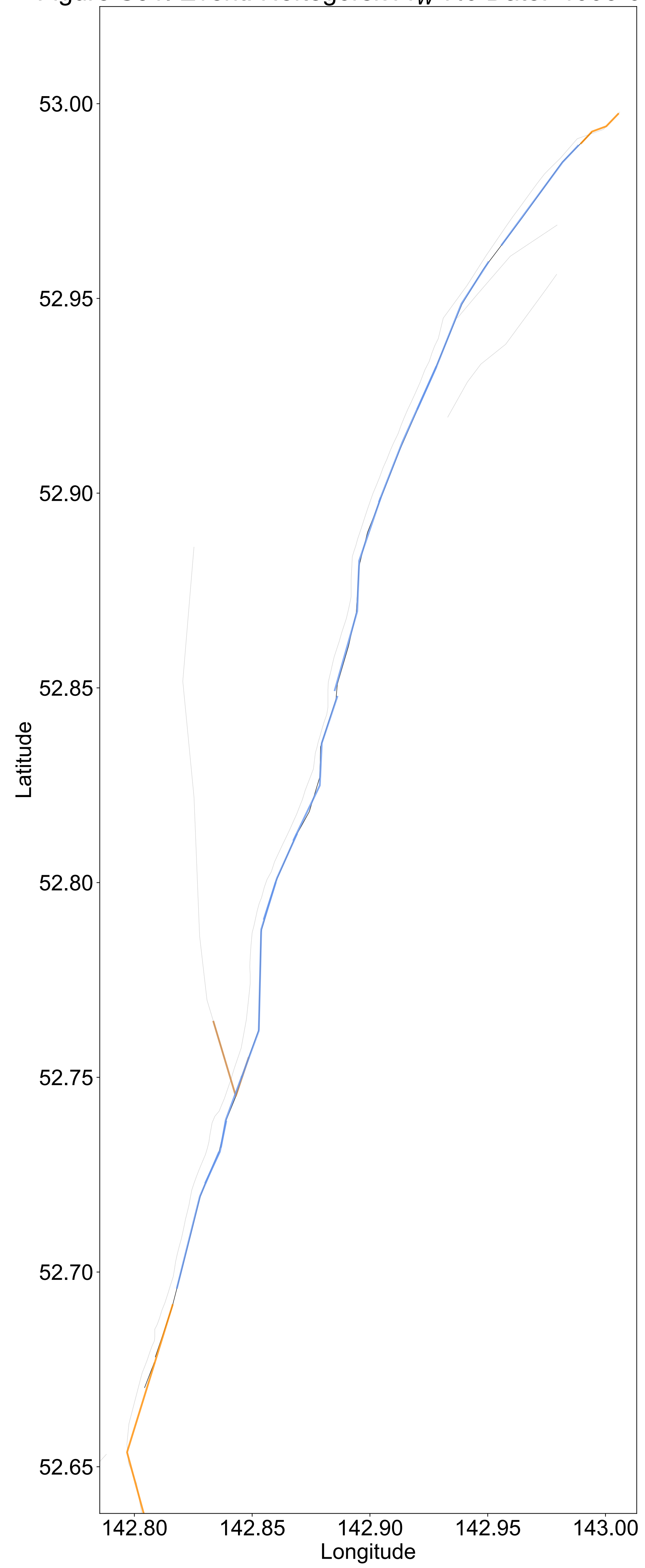


Figure S32. Event: Kobe M_W 6.9 Date: '1995-01-16'

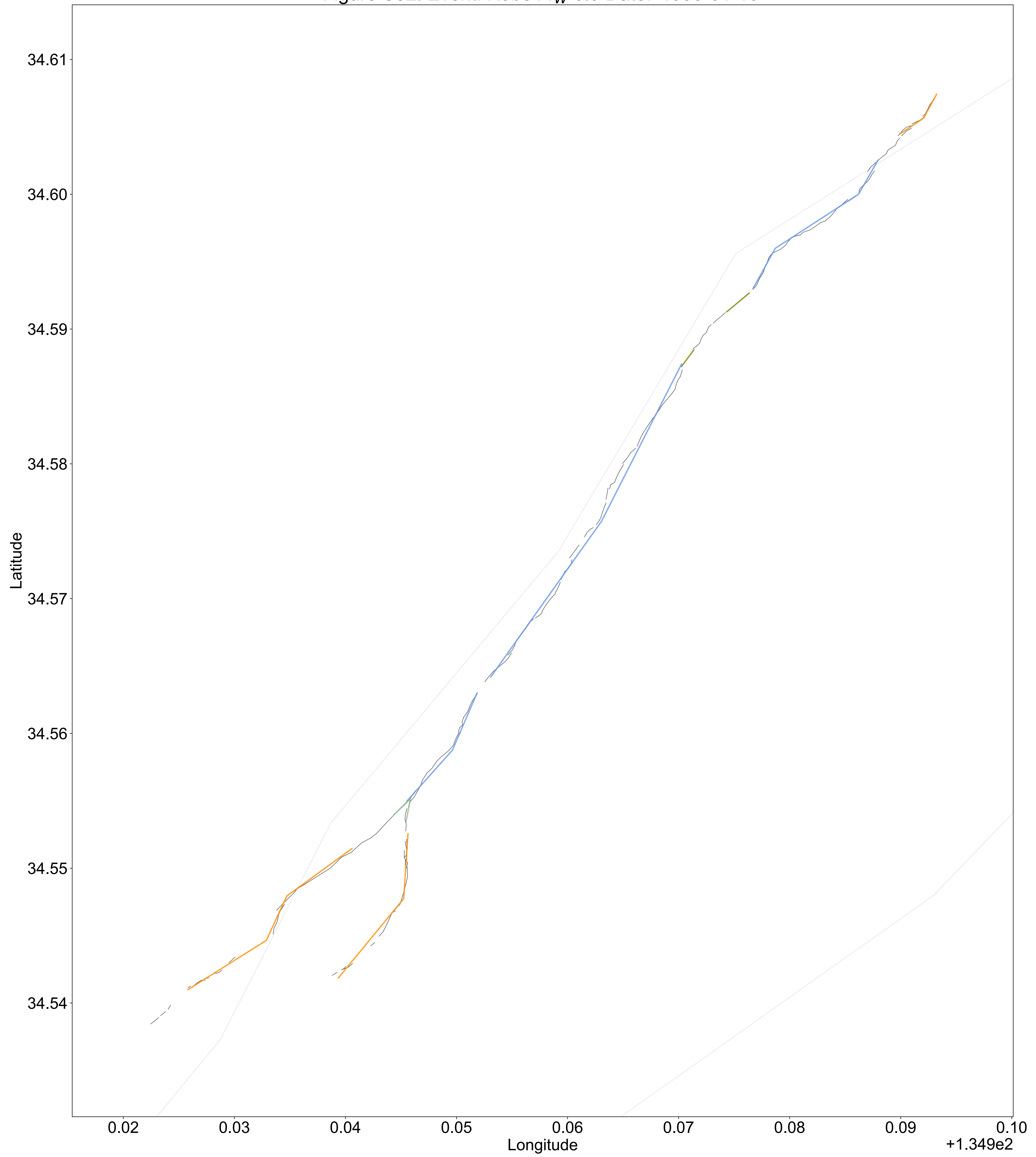


Figure S33. Event: Parkfield2004 M_W 6.0 Date: '2004-09-28'

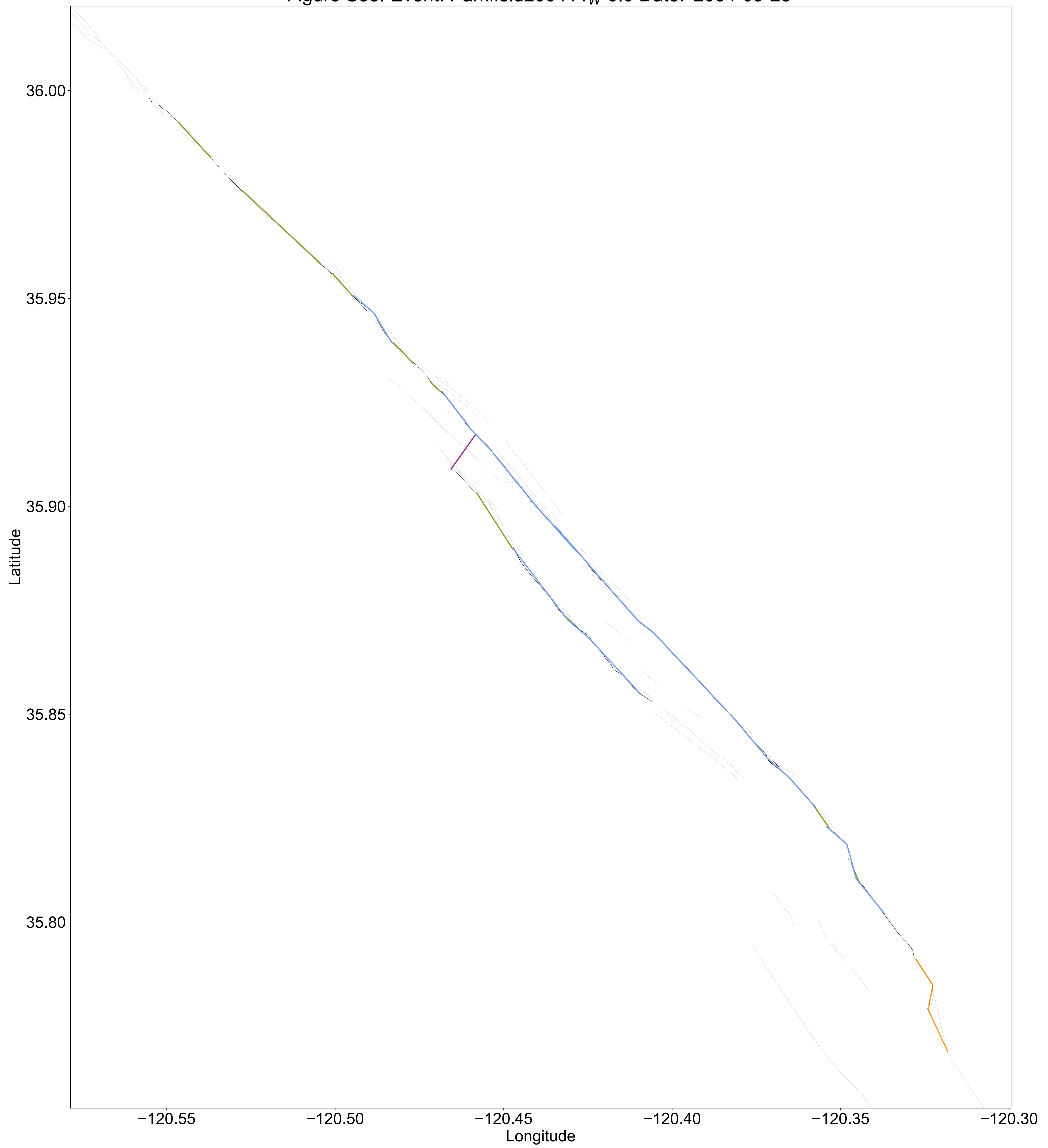


Figure S34. Event: SuperstitionHills M_W 6.54 Date: '1987-11-24'

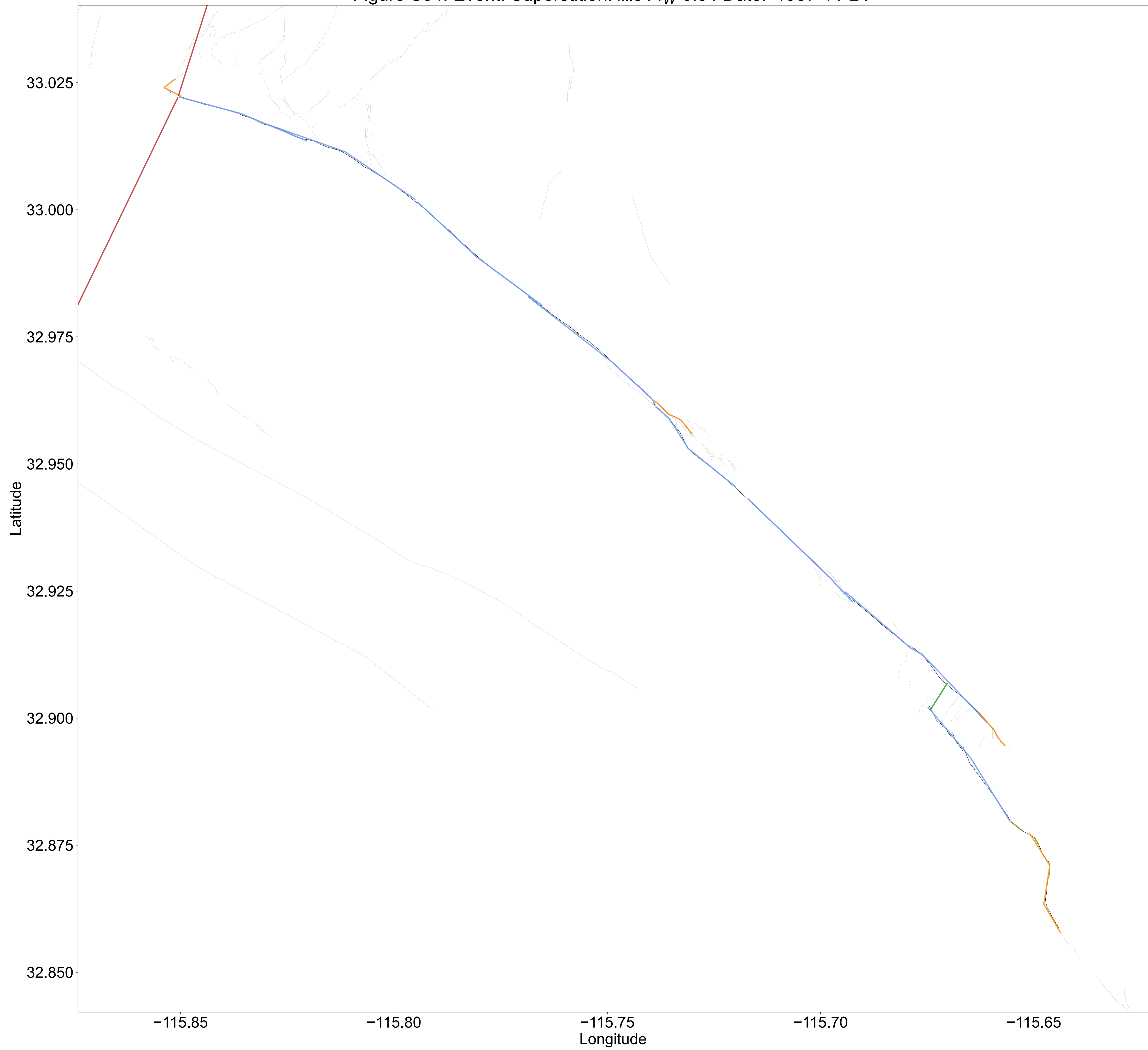


Figure S35. Event: Duzce M_W 7.14 Date: '1999-11-12'

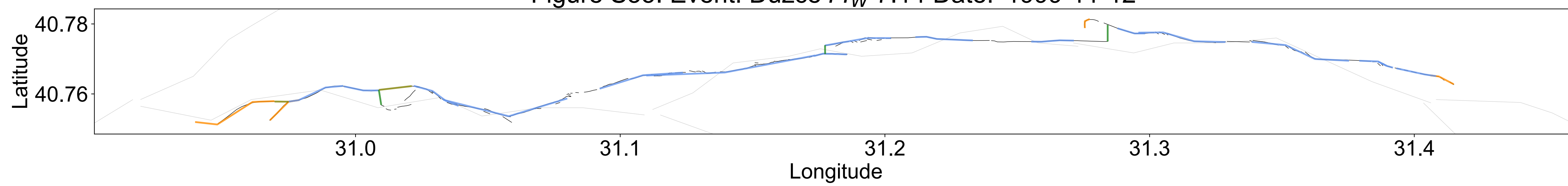


Figure S36. Event: Imperial1940 M_W 6.95 Date: '1940-05-19'

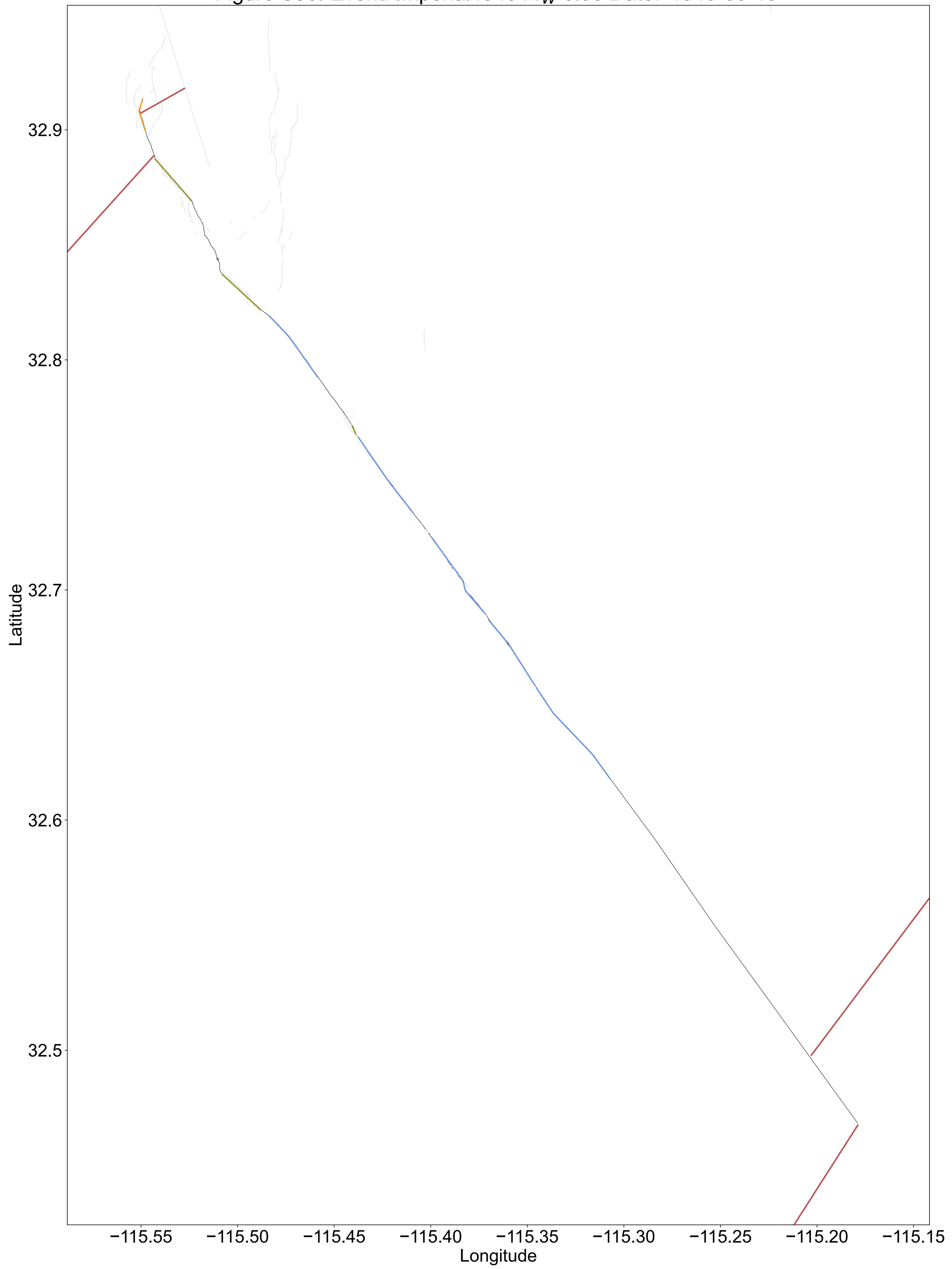


Figure S37. Event: GalwayLake M_W 5.2 Date: '1975-06-01'

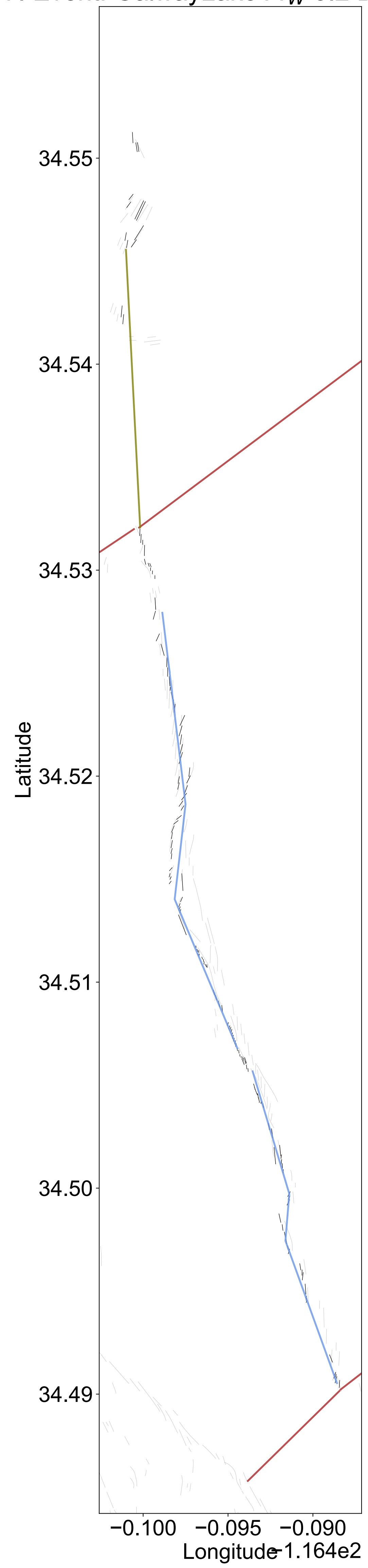


Figure S38. Event: Hualien M_W 6.4 Date: '2018-02-06'

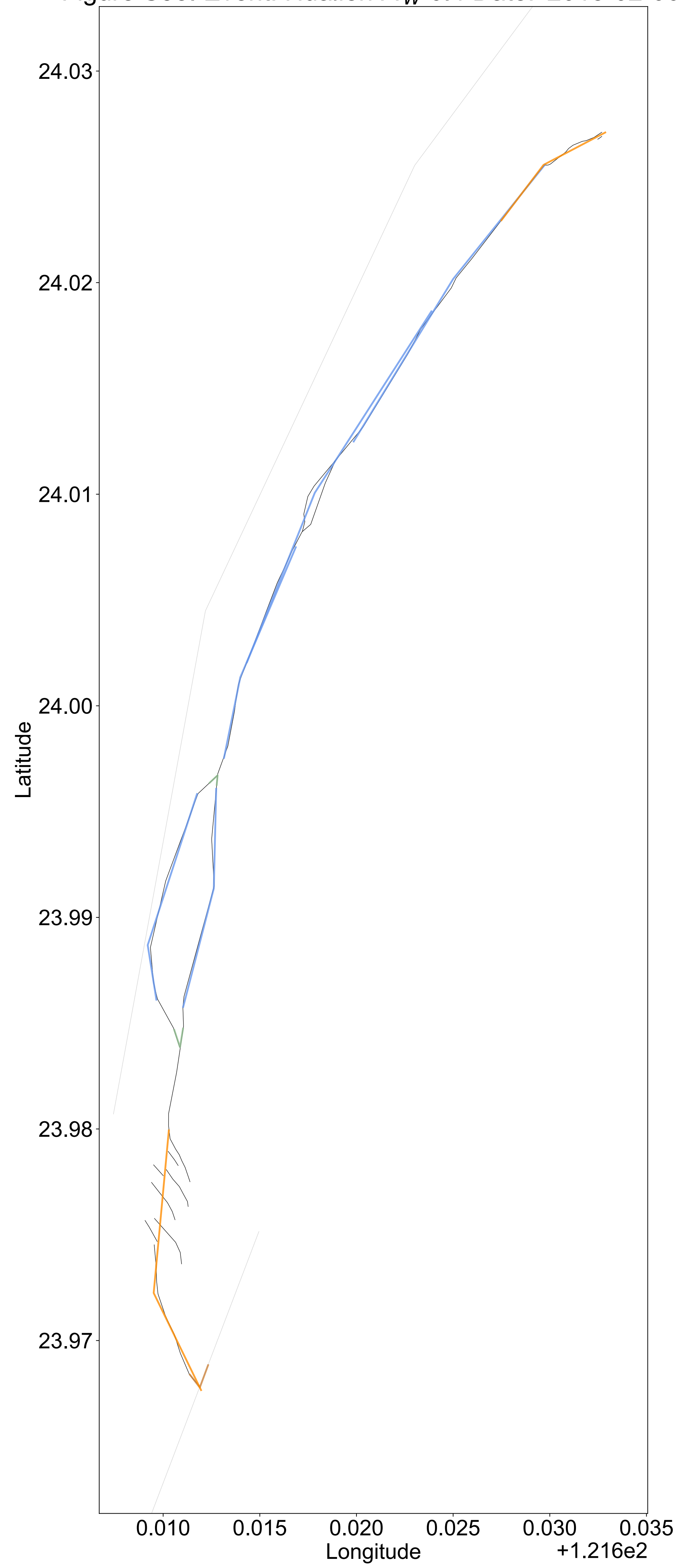


Figure S39. Event: Izmit M_W 7.51 Date: '1999-08-17'

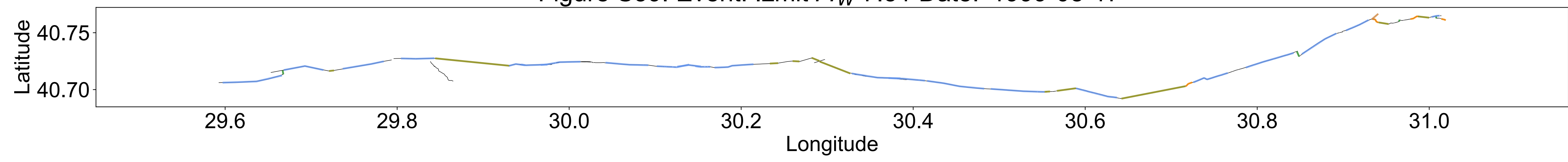


Figure S40. Event: Ridgecrest1 M_W 6.4 Date: '2019-07-04'

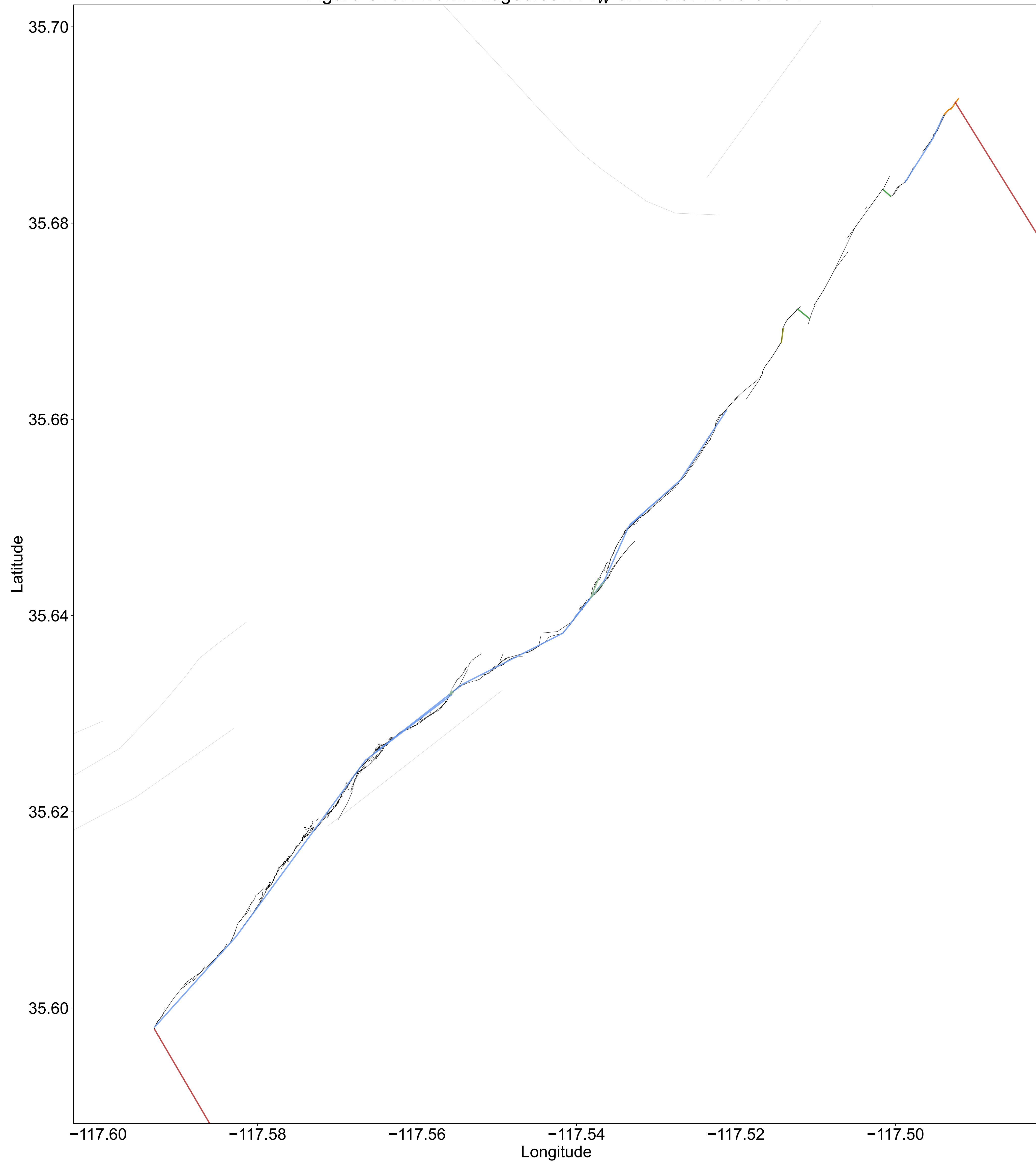


Figure S41. Event: IzuPeninsula M_W 6.5 Date: '1974-05-08'

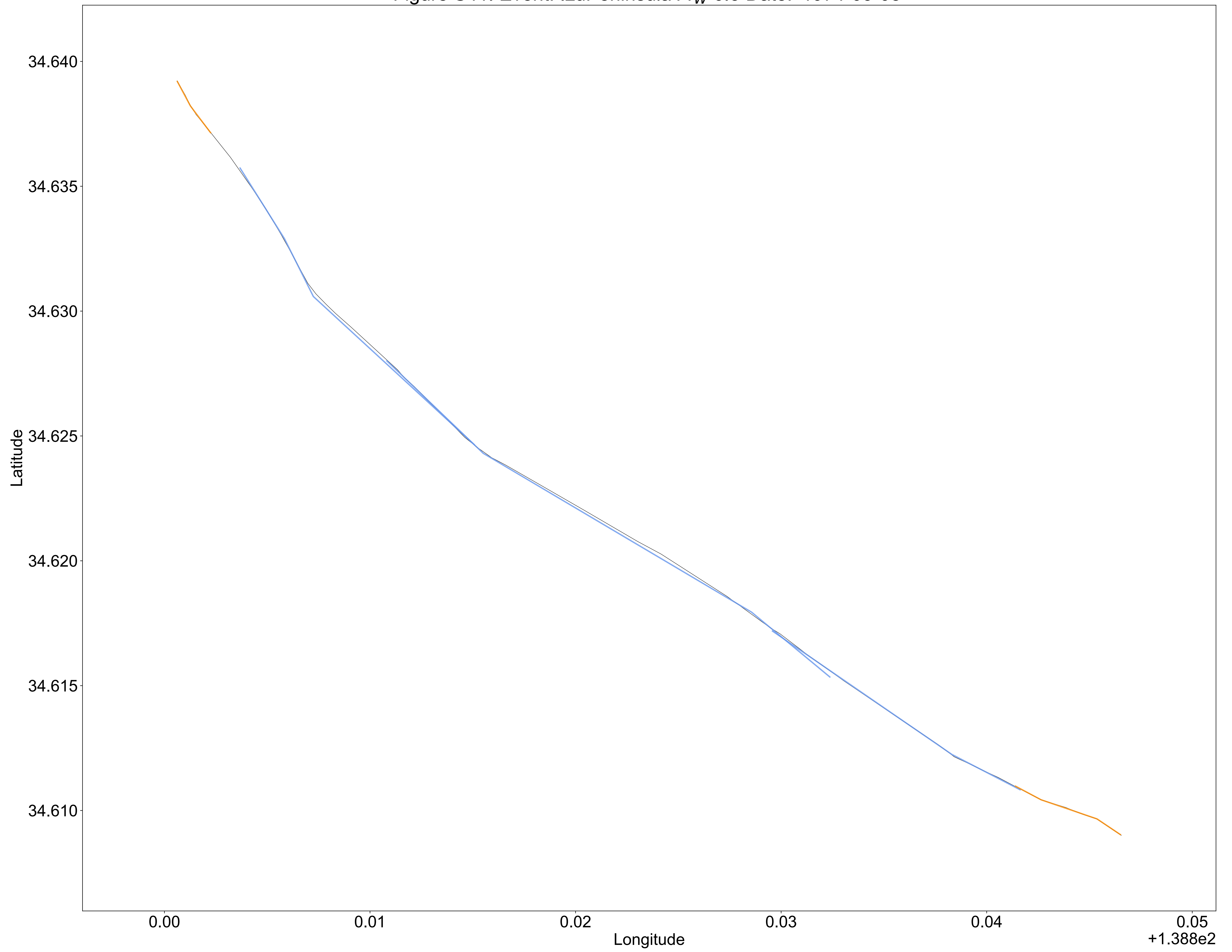


Figure S42. Event: Luzon M_W 7.7 Date: '1990-07-16'

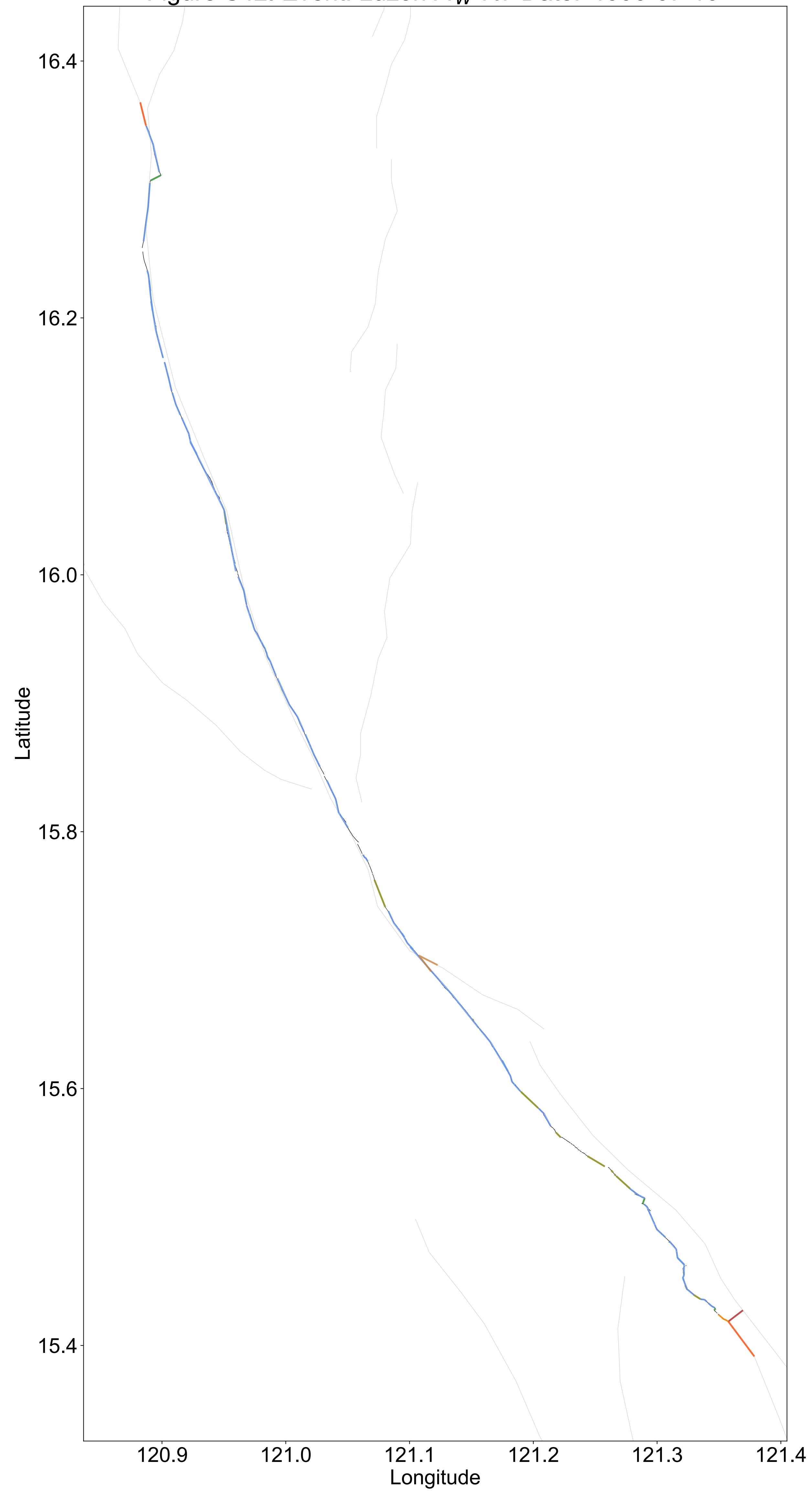


Figure S43. Event: Kumamoto M_W 7.0 Date: '2016-04-15'

